



UNIVERSIDAD  
DE LA REPUBLICA  
URUGUAY



# Numerical simulation of wind farms

## Operation of wind turbines under power restrictions imposed by the electric grid

Andrés Guggeri Solaro

Postgraduate Program in Energy Engineering  
School of Engineering  
Universidad de la República

Montevideo – Uruguay  
January 2019





UNIVERSIDAD  
DE LA REPUBLICA  
URUGUAY



# Numerical simulation of wind farms

Operation of wind turbines under power restrictions  
imposed by the electric grid

Andrés Guggeri Solaro

Master's Thesis presented to the Postgraduate program in Energy Engineering, from the School of Engineering at the University of the República, Uruguay, as a requisite for acquiring a Master degree in Energy Engineering.

Director:

D.Sc. Prof. Gabriel Usera

Co-advisor:

D.Sc. Prof. Martín Draper

Academic director:

D.Sc. Prof. Gabriel Usera

Montevideo – Uruguay

January 2019



Guggeri Solaro, Andrés

Numerical simulation of wind farms / Andrés Guggeri Solaro. - Montevideo: Universidad de la República, Facultad de Ingeniería, 2019.

XXII, 66 p. 29, 7cm.

Director:

Gabriel Usera

Co-advisor:

Martín Draper

Director académico:

Gabriel Usera

Tesis de Maestría – Universidad de la República, Programa en Ingeniería de la Energía, 2019.

Referencias bibliográficas: p. 65 – 66.

1. Mecánica de Fluidos Computacional, 2. Energía Eólica, 3. Control de potencia aerogeneradores, 4. Restricción de potencia. I. Usera, Gabriel, *et al.* II. Universidad de la República, Programa de Posgrado en Ingeniería de la Energía. III. Título.



EXAMINING COMMITTEE

---

D.Sc Prof. Federico Favre

---

Ph.D Prof. Filippo Campagnolo

---

M.Sc. Eng. Ruben Chaer

Montevideo – Uruguay  
January 2019



A mis padres



# Agradecimientos

Estoy muy contento de haber llegado a esta etapa, que marca la culminación del trabajo de Tesis así como de la Maestría, la cual disfruté mucho.

En primer lugar agradezco a Martín, que me acompañó y guió a lo largo de este camino, de quien aprendí y sigo aprendiendo acerca de mecánica de fluidos, energía eólica y también de la vida. Tus consejos, ideas, paciencia, y aclaraciones de dudas (en muchos casos generando nuevas!) me dieron mucha motivación para realizar este trabajo, gracias! A Gabriel, siempre dispuesto a dar una mano, comprensivo y con soluciones muy creativas y útiles cuando nos enfrentábamos a algún problema, también te digo muchas gracias. Le agradezco a mis seres queridos, mi familia, mi novia María Emilia, y mis amigos de Salto, a su manera todos me han motivado y apoyado desde el primer momento, para que realice esta Maestría y hoy pueda terminarla.

Ahora paso a agradecer a esas personas que están todos los días, mis compañeros de oficinas, tanto del IMFIA como de Ventus. Gracias amigos de la 234 y 236, por el buen ambiente que tenemos en la oficina, con nuestras charlas (de ingeniería y otros variados temas), cafe, mates, los almuerzos, sin duda que es una motivación diaria. Respecto a Ventus, agradezco a la barra del piso 3, con quienes he compartido muy buenos momentos a lo largo de estos dos años, en particular al equipo de OyM, quienes me dieron muy buenos consejos y transmitieron sus conocimientos acerca del funcionamiento de los aerogeneradores. Igualmente, gracias a la empresa Ventus, por su disposición a compartir datos e información de parques eólicos, los cuales resultaron muy útiles para validación del modelo.

También estoy muy agradecido a los profesores encargados de los cursos de la Maestría, de quienes adquirí muchos conocimientos de temas relacionados a la energía, y que además contribuyeron a lidiar con problemas de esta tesis.

Finalmente, agradezco a la Agencia Nacional de Investigación e Innovación por su confianza al concederme una Beca para la realización de esta Maestría.



(Epigraph:) *I am among those  
who think that science has great  
beauty.*

Marie Curie



## ABSTRACT

This thesis deals with the operation and power production of wind farms, focusing on active power control of wind turbines. This work is carried out by means of numerical simulations with a Computational Fluid Mechanics approach. The wind field dynamics equations are solved using the numeric code `caffa3d`, with a Large Eddy Simulation framework and the Actuator Line Model to represent the wind turbine rotors. A torque-generator controller and closed-loop Proportional-Integral collective pitch controller were implemented in `caffa3d` code, with the purpose of following an active power signal determined by the operator. These models enable to simulate the operation of wind turbines subject to the entire range of wind velocity and contributes to reproduce in a more precise way the real behavior of the turbine, allowing to find both qualitative and quantitative results of the interaction between the wind flow and the turbines.

To validate the simulations, the results were compared with experimental data of the wind field and the operation of wind turbines, obtained from two sources: the 7.7MW onshore wind farm, 'Libertad', located in Uruguay; and a wind tunnel campaign of a wind farm. The results obtained in the simulations are consistent with the experimental ones, so the state of the art is considered to be reached in order to simulate the operation of turbines and their power control at individual level. The comparison was focused in integral quantities, in particular active power, as well as in the rotor angular velocity, blade-pitch angle and wind speed. Simulations of different wind speed and direction situations were carried out, also considering different signals of active power, evaluating the characteristics of the wakes, the operation of the turbines and the total production of the wind farm.

Keywords:

Computational Fluid Dynamics, Wind Energy, Active power control, Power restriction.



## RESUMEN

Esta tesis trata sobre la operación y la producción energética de parques eólicos, centrándose en el control de la potencia activa de los aerogeneradores. Este trabajo se realiza mediante simulaciones numéricas con foco en la Mecánica de Fluidos Computacional. Las ecuaciones de la dinámica de campo de viento se resuelven utilizando el código numérico `caffa3d`, en el marco de Simulación de Grandes Vórtices junto con el Modelo de la Línea Actuadora para representar los rotores de las turbinas eólicas. Se implementaron en el código un controlador de torque eléctrico y un controlador de ángulo de pala de lazo cerrado, con el propósito de seguir una señal de potencia activa determinada por el operador. Estos modelos permiten simular el funcionamiento de turbinas eólicas sujetas a todo el rango de velocidad del viento, contribuyendo a reproducir de una manera más precisa su comportamiento real.

Para validar las simulaciones, los resultados se compararon con datos experimentales de campo de viento y operación de los aerogeneradores, obtenidos de dos fuentes: el parque eólico de 7.7MW, 'Libertad', ubicado en Uruguay; y una campaña en un túnel de viento de un parque eólico a escala. Los resultados obtenidos en las simulaciones son consistentes con los experimentales, considerando así que se ha alcanzado el estado del arte para simular el funcionamiento de las turbinas y su control de potencia a nivel individual. La comparación se centró en cantidades integrales como potencia activa y torque, además de velocidad angular del rotor, ángulo de pala y la velocidad del viento. También se llevaron a cabo simulaciones de otras situaciones de velocidad y dirección del viento, y variadas señales de potencia activa, evaluando las características de las estelas, la operación de las turbinas y la producción total de parque.

Palabras claves:

Mecánica de Fluidos Computacional, Energía Eólica, Control de potencia aerogeneradores, Restricción de potencia.



# Acronyms

**ABL** atmospheric boundary layer 7, 8

**ALM** Actuator Line Model 6, 7

**CFD** Computational Fluid Dynamics 4

**NIS** National Interconnected System 2

**SCADA** Supervisory Control And Data Acquisition 5, 6, 7, 8, 9

**TUM** Technische Universität München 5, 7

**WF** Wind Farm 2, 3, 5, 6, 7, 8, 9

**WT** Wind Turbine 1, 2, 4, 6, 8, 9



# Contents

<b>Acronyms</b>	<b>XIX</b>
<b>1 Introduction and Overall Conclusions</b>	<b>1</b>
1.1 Motivation . . . . .	1
1.2 Objectives . . . . .	3
1.3 Methodology . . . . .	4
1.4 Structure . . . . .	5
1.5 Papers review . . . . .	6
1.5.1 Paper 1 . . . . .	6
1.5.2 Paper 2 . . . . .	7
1.5.3 Paper 3 . . . . .	7
1.5.4 Paper 4 . . . . .	8
1.6 Overall conclusions and future work . . . . .	9
<b>2 Papers</b>	<b>11</b>
2.1 Paper 1: Simulation of a 7.7 MW onshore wind farm with the Actuator Line Model . . . . .	11
2.2 Paper 2: A High-Fidelity Numerical Framework For Wind Farm Simulations . . . . .	22
2.3 Paper 3: An Actuator Line Model Simulation of two semi- aligned wind turbine models, operating above-rated wind speed	36
2.4 Paper 4: Actuator Line Model simulations to study active power control at wind turbine level . . . . .	51
<b>Bibliography</b>	<b>65</b>



# Chapter 1

## Introduction and Overall Conclusions

### 1.1. Motivation

The generation of energy through renewable resources has had a great expansion in recent decades worldwide, driven by various causes. Among them is the high volatility of non-renewable resource markets, such as fossil or nuclear fuels, which has a direct impact on the cost of electricity, mainly in countries that do not have these resources and depend on their import, which motivates diversifying the energy matrix to avoid this dependence. There is also a growing awareness and concern about global warming and its possible consequences in the future. Generating energy with renewable sources has a very low carbon footprint compared to technologies that use fossil fuels, so they emit lower amounts of greenhouse gases, one of the main causes of global warming; they also require much less water to generate to produce electricity than fossil fuel or nuclear power plants. It is also important to highlight the technological advance of renewable generation, especially the traditional ones, wind and solar energy. This has significantly impacted both the reduction of its costs and improvements in performance, which makes its economic equation more attractive [1].

Within renewable energies, large horizontal axis Wind Turbine (WT) is the technology with the fastest and greatest development in the past decades, with an exponential growth rate [2]. A characteristic of WT is their ability to control the power output, when they are subject to spacial and temporal variations of

the wind speed flow, and as consequence to the variation of the forces acting on the rotor. The conventional approach to accomplish this is the design of two control systems which work independently, at the below-rated and above-rated wind-speed range [3]. These systems are the generator-torque controller, whose objective is to maximize power capture below the rated operation point, and the rotor-collective blade-pitch controller, with the goal of regulating the generator speed, and thus the rotor angular speed, at the rated operation point.

In addition to the advantages previously mentioned, there are several reasons that motivate the installation of wind turbines to generate electricity [1], among which the following stand out:

- Unlike conventional hydraulic or thermal power plants, the construction, installation and commissioning of a large-scale Wind Farm (WF) can be done in a short time, of the order of a few years
- The relationship between surface used and generated energy is very low. The power of each WT can reach several Megawatts (MW), which leads to having wind farms of tens or hundreds of MW, where in turn you can use the soil between the wind turbines for another activity.

In particular, Uruguay has had a great development in the incorporation of this technology to its energy matrix in the last decade, and the reasons do not escape to previously enumerated. Currently, there are more than 1500MW of installed wind power, with the peak demand of the order of 2000MW 4. This, added to the installed capacities of solar, biomass and hydraulics make a total of more than 90 % of installed power, placing Uruguay as one of the countries with the highest generation of electric energy by renewable sources in the world. In of March 2018, for the first time in the history of the country, wind power was the main source of electricity generation, reaching a 41 % share [5].

However, having a high participation of wind in the electric energy matrix also has disadvantages, with one of the most significant being the random occurrence of the wind resource due to its nature. As for the moment large scale energy storage forms have not been developed in Uruguay, beyond the lakes corresponding to the hydroelectric power plants, the WF operate always delivering to the network the maximum power that is available whenever it is required. In turn, current wind turbines have power electronics technology, which implies, among other things, that wind farms are electrically uncoupled

to the network. Although WF are able to contribute or consume both active and reactive power, according to the requirements of the National Interconnected System (NIS) operator, they do not respond in the same way to changes in the operating variables of the electrical grid, such as frequency, than conventional power plants. All this generates inconveniences for the operator of NIS, since the uncertainty in the planning of the dispatch increases and it is more difficult to maintain the stability of the system. To mitigate these problems, electric energy dispatch office has forecasts of the wind resource of different time horizons, in the order of hours and days, which are considered to plan the dispatch. Despite this, there are situations in which it is required to limit the active power supplied by a WF. Examples of this are some nights when the demand for energy is low and the wind resource is high, or when the electric power lines do not support more power. This requirement active power is constantly being received by the WF, and it is fulfilled by modifying the operation of each turbine, regulating its operating parameters, such as pitch and/or speed of rotation.

## 1.2. Objectives

The main objective of this Thesis is to numerically simulate the operation of a WF subject to an active power limitation. The research seeks to obtain an adequate representation of the operation of the turbines, both from the qualitative and quantitative point of view. It is expected that this development will contribute to reproduce in a more precise way the real behavior of the turbines and that enables to simulate other situations, either in project or operational stages, through a validated and high fidelity tool.

Specifically, the objectives are:

- Analyze and model the regulation of the operating parameters, electric torque and collective pitch angle, oriented to power control.
- Implement in the code a power controller for individual wind turbines, with the objective of simulating operating situations under the previously mentioned restrictions.
- Assess the capacity of the numerical tool to model the operation of single wind turbines as well as the whole farm, analyzing the time evolution of the variables involved and the capacity of the WF to generate a fixed

power value determined by the operator.

### 1.3. Methodology

This Thesis aims to address the operation of wind turbines under an power constraint, with a Computational Fluid Dynamics (CFD) approach. The great increase in the processing power of computers and the development of parallel calculations have allowed designing adequate numerical models for the simulation and resolution of various situations. In particular, CFD codes have a crucial role, suitable for solving the dynamics of a flow in intricate geometries and their interaction with obstacles. Not surprisingly, many of the advanced research projects, both academic and industrial, use CFD tools in a wide variety of subjects, from micro-scales for example for the study of combustion in engines, to macro-scales for global climate studies. There are also applications for these simulations in sports, transport system design, turbo-machine studies, dispersion of pollutants in urban environments, among many others. A series of accurate simulations can be a convenient way to produce useful data, mainly because it is more cost-effective when compared to experiments performed in real physical environments, such as wind tunnels or field measurements.

In this sense, the use of CFD codes for the simulation of wind fields of atmospheric boundary layer type and their interaction with WT constitutes the state of the art, presenting potential applications during the useful life of a wind farm. The CFD used in this work is `caffa3d` [6] [7], an open source, finite volume (FV) code with second order accuracy in space and time, parallelized with MPI, in which the domain is divided in unstructured blocks of structured grids. Two approaches exist in order to represent the presence of a WT in a simulation: 1) actuator models, in which the blades are represented as body forces and 2) direct representation of the blade's geometry through the computational mesh. As the second approach implies a very high computational costs when applied to wind farm scales, the first approach is chosen. The implementation and validation of actuator disk (with and without rotation) and actuator line models in `caffa3d` solver is presented in [8] [9] [10].

In the present work, the power control of WT was modeled and implemented in CFD `caffa3d.MBRi` code, by means of the regulation of their operating parameters, such as blade-angle (pitch) and speed of rotation. To carry out the numerical simulations the intensive computing service of the School of Engi-

neering, Cluster-FING, was used. This infrastructure is composed of more than 25 computing servers equipped with modern Intel Xeon and AMD processors Opteron with a total of more than 500 cores of computation, 1 TB of RAM and more than 200TB of disk space, being interconnected by networks Gigabit and 10-Gigabit, which allows executing models integrated by more than 100 million computing cells based on massively parallel computing strategies in distributed memory. Currently the computations are migrating to the National Computing Center (ClusterUy), a computer service which belong to some state companies, as well as the the School of Engineering . This recently inaugurated infrastructure works through the aggregation of hardware components that are able to work cooperatively as a single integrated computing resource, under the cluster model, with a platform which integrates 1312 CPU counting cores and 100352 GPU computing cores, with a theoretical peak performance of 720 TFlops (<http://cluster.uy/>).

To validate the model, the results of the simulations are compared with data obtained from two sources: from the Supervisory Control And Data Acquisition (SCADA) data of the WF Libertad wind farm, located in Uruguay; from experimental data obtained in a test of 2 turbine models in a wind tunnel, carried out by the Wind Energy Institute of Technische Universität München (TUM).

## 1.4. Structure

During the development of this thesis, seeking to meet the previously mentioned objectives, the advances in the work were collected in scientific articles for presentation at conferences on the subject. This process concluded in the writing of 4 articles [11] [12] [13] [14], the first one presented in the 'Wake Conference 2017', the second and third ones at 'The 10th International Conference on Computational Fluid Dynamics'. The fourth paper was proposed for the 'Wake Conference 2019' and is currently under review. The presented articles were published in the proceedings of the respective conferences. Each one constitutes a self-contained work, which includes its corresponding review of the state of the art, description of the methodology, validation of results and main conclusions. Without detriment of the above, the 4 articles are related, with this relationship being the thread of the Thesis, and their conjunction make the totality of this work.

## 1.5. Papers review

A brief description of the content of each article is made below, and overall conclusions and future work are proposed in the final section of this introduction

### 1.5.1. Paper 1

The objective of this work was to study the interaction between wind turbines due to their wakes, continuing the evaluation of Actuator Line Model (ALM) when it is used with coarser resolution and larger time steps than what is recommended when simulating an actual WF. To this end, the 7.7MW onshore wind farm 'Libertad' was simulated, considering several wind directions, and the results were compared with SCADA data from the turbines and the meteorological tower. The WF consists of 4 Vestas V100 wind turbines, a description of the WF is given, as well as the numerical configuration applied to represent it, including the used resolutions. The paper presents the methodology used to estimate the geometry and aerodynamic coefficients of the V100 wind turbine, using on the Blade Element Momentum method. For these simulations, the pitch controller was not yet implemented, so that variable was considered constant throughout the simulation, while the speed of rotation is regulated by looking directly at tabulated values, depending on the aerodynamic torque of each temporary step. The wind profile considered at the input of the numerical domain was computed previously with a precursor simulation, which had periodic boundary condition at the east and west boundaries, did not include wind turbines and had the same spatial resolution than the simulation which includes WT. The wind profile had an average speed at hub height lower than the rated of the turbines, so the fixed value of the blade angle is kept constant at its minimum, which is  $-2^\circ$ .

The article shows results of simulations considering two wind directions in which there is interaction between wind turbines and their wakes. The power results are compared with 10-minute data obtained from the SCADA of the turbine, using the values of wind speed and wind direction registered by the meteorological tower to filter the mentioned data. For this comparison, the average power obtained from simulations of three/five wind directions is computed, in order to account for narrow/wide wind direction sector, and compare it with the SCADA data. Acceptable agreement is found in the com-

parison, SCADA with the simulations being able to represent the power deficits of speed that are appreciated in the SCADA data. A sensitivity analysis of the power results with respect to the spatial resolutions was performed, finding significant differences in the results obtained with each of the three resolutions. The explanation for this was that for each case a different precursor simulation was computed, as the resolutions of the precursor simulations and the simulations with WTG must be the same. This caused the velocity upstream the wind turbines and meteorological tower was slightly different in each case, despite having almost the same velocity profile averaged in the spanwise direction, and this impacted in the power results.

### **1.5.2. Paper 2**

This second paper has a similar approach and objective with respect to the previous one, focusing on the interaction between wind turbines and their wakes. The same wind farm, Libertad, is simulated, evaluating the power and velocity deficits as well the total WF production, although in this work subject to 14 different wind directions. To accomplish this, a procedure to automatize the simulation's setup was implemented with a Matlab script, which rotates and crop the domain according to the given wind direction, domain size and resolution, then generate the grids, set-up the simulation and sends it to be computed at the cluster. As in the previous paper, the results are compared with SCADA data, which contains an extra year of information than the previous work, also considering the power mean value among two wind directions.

In this work the pitch controller was already implemented, but the paper did not focused on it, as at most of the simulation time it was not active. This occurred because the atmospheric boundary layer (ABL) wind velocity profile considered at the inlet was below rated, so rated angular speed was rarely reached and thus the pitch-angle was kept constant at its minimum value. A detailed description of the torque generator and pitch and its validation is given in the following papers.

### **1.5.3. Paper 3**

In this work the numerical method is applied for the simulation of two model wind turbines operating at above rated wind speed. The model wind turbines, called G1, belong to the Wind Energy Institute of TUM, who ha-

ve tested them in several wind tunnel campaigns, subject to different inflow conditions and operational modes. The implementation and validation of their characteristics in the ALM of `caffa3d` was previously presented in [15], comparing the results with data from one of this experimental campaigns.

As it was mentioned, a basic characteristic of WT is their ability to limit their power production when the wind speed is greater than the rated one. To represent this in the numerical simulations, a generator-torque and closed-loop pitch controller were implemented in the code. The operation of the turbines was simulated subject to five different ABL wind velocity profiles at the inlet of the domain. The results of one simulation are compared to data obtained from a wind tunnel campaign, showing the expected performance of the turbines to control their power output. We found good agreement between the temporal evolution of the involved variables as well as mean values of integral quantities, such as the power coefficient.

#### **1.5.4. Paper 4**

This last paper is based on what was implemented in the previous works, with the objective of simulating the operation of a wind farm subject to different power restrictions. To this end, the paper presents the implementation of the power controllers for the Vestas V100 WT model, describing the methodology applied to obtain the controller parameters and a method to operate the WT in de-rate mode, that it producing less than its rated value. The 'Libertad' WF was simulated, subject to two different ABL wind velocity profiles, above and below rated; two wind directions, with and without interaction of WT and their wakes, and several de-rate values, both constant and time varying.

SCADA data of the WF acquired at high frequency (1Hz) is compared with some simulation results, in order to validate them. The paper discussion focus on the temporal evolution of the following signals: wind velocity, rotor speed, angular speed, electric and aerodynamic torque and power. Also a simulation of single wind turbine with plain topography is preformed, considering different de-rate values, with the purpose of evaluate the wind velocity deficit on its wake.

## 1.6. Overall conclusions and future work

A Large Eddy Simulation framework with the Actuator Line Model to represent the wind turbine rotors has been used to simulate the operation of a full-scale WF and a scaled wind energy facility. A torque-generator controller and closed-loop Proportional-Integral (PI) pitch controller were implemented in `caffa3d` code, as a series of subroutines in already existing modules. The main conclusion of this work is that the model is now capable of simulating the operation of WT subject to the entire range of wind velocity, which contributes to reproduce in a more precise way the real behavior of the turbines. This way, the state of the art to simulate the operation of turbines and their power control at individual level is reached in order, and the objective of the Thesis is accomplished.

In order to validate the simulation results, the mean values as well as the temporal evolution of the variables were compared to SCADA data of real WF and experimental data from a wind tunnel campaign. The comparison was focused in integral quantities, in particular active power, as well as in the rotor angular velocity, blade-pitch angle and wind speed, and in the interaction between WT and their wakes was also analyzed. For the two simulated cases, good agreement both in the mean values and the temporal evolution of the signals were found, results that are also in accordance with what was expected according to the bibliographic review. Particular observations regarding numerical results, their uncertainties and some differences with experimental data, are made on each paper.

As a particular conclusion, it is shown that when there is enough wind power, the individual wind turbines can follow the required signal, but when looking at the total wind farm power output, it fails to accomplish what is required, particularly because of the interaction between wakes and turbines. This result shows the necessity of implementing a global controller, which takes into account the available power of the wind turbines, and distributes an active power reference to each one. To accomplish this, further investigation to estimate the free wind velocity up-stream of a WT as well as on the wakes characteristics is needed.



## Chapter 2

### Papers

- 2.1. Paper 1: Simulation of a 7.7 MW onshore wind farm with the Actuator Line Model

# Simulation of a 7.7 MW onshore wind farm with the Actuator Line Model

**A Guggeri, M Draper, G Usera**

Universidad de la República, Facultad de Ingeniería, Julio Herrera y Reissig 565 11300, Montevideo, Uruguay

E-mail: [aguggeri@fing.edu.uy](mailto:aguggeri@fing.edu.uy), [mdraper@fing.edu.uy](mailto:mdraper@fing.edu.uy), [gusera@fing.edu.uy](mailto:gusera@fing.edu.uy)

**Abstract.** Recently, the Actuator Line Model (ALM) has been evaluated with coarser resolution and larger time steps than what is generally recommended, taking into account an atmospheric sheared and turbulent inflow condition. The aim of the present paper is to continue these studies, assessing the capability of the ALM to represent the wind turbines' interactions in an onshore wind farm. The 'Libertad' wind farm, which consists of four 1.9MW Vestas V100 wind turbines, was simulated considering different wind directions, and the results were compared with the wind farm SCADA data, finding good agreement between them. A sensitivity analysis was performed to evaluate the influence of the spatial resolution, finding acceptable agreement, although some differences were found. It is believed that these differences are due to the characteristics of the different Atmospheric Boundary Layer (ABL) simulations taken as inflow condition (precursor simulations).

## 1. Introduction

Wind energy has expanded rapidly in recent decades all over the world. The increase in wind power in 2015 was close to half of global electricity generation growth and wind power capacity increased by 17% from 2014 to 2015 [1]. The growth rates have become lower in recent years, nevertheless the installed capacity is projected to increase in the following years [2]. This development of wind energy has been supported by technological improvements which are related to an increase in hub height, rotor diameter and unit power, which has led to larger capacity factors for the same wind speed [3]. This growth in size means, among other things, that the area of interest of the atmospheric boundary layer (ABL) swept by these wind turbine rotors, reaches higher altitudes and it is placed further away from the surface. It also means that the influence of different atmospheric conditions, such as turbulence intensity and vertical velocity gradient, in the wake of a wind turbine and in its performance, is larger [4][5][6][7].

Two approaches exist in order to represent the presence of a wind turbine in a simulation [8]: 1) actuator models, in which the blades are represented as body forces, 2) direct representation of the blade's geometry through the computational mesh. The Actuator Line Model (ALM) has been widely validated [9][10][11][12][13][14], showing to reproduce with reasonable accuracy the wind flow in the wake of a wind turbine with moderate computational cost. In general, it is recommended to use a spatial resolution of at least  $R/30$ , being 'R' the rotor radius, and to limit the movement of the rotor tip to a grid cell length in each time step [14]. Recently, the ALM has been evaluated with coarser resolutions and also larger time steps, considering a uniform inflow condition [15] as well as an Atmospheric Boundary Layer (ABL) like inflow condition. For the latter the 'Horns Rev' offshore wind farm and a well-known wind



tunnel campaign, were considered as validation cases [16][17], finding good agreement with the SCADA data in the power deficits in [17] and accuracy to reproduce the wake of the wind turbine in [16].

The aim of the present paper is to continue the research done in the past years, analyzing the power produced by the turbines and the influence of the wakes. For this, ‘Libertad’ onshore wind farm was simulated, considering different wind speeds and wind directions. The paper is organized as follows: Section 2 presents the solver and the ALM implementation, Section 3 describes the validation case used for the evaluation and the numerical setup, Section 4 presents the main results, discussing the effect of considering three different resolutions, and summary is given in Section 5.

## 2. Numerical method

### 2.1. Solver

caffa3d.MBRi [18] [19] is an open source, finite volume (FV) code, with second order accuracy in space and time, parallelized with MPI, in which the domain is divided in unstructured blocks of structured grids. Representation of complex geometries can be handled through a combination of body fitted grids and the immersed boundary method over both, Cartesian and body fitted grid blocks. Geometrical properties and flow properties, which are expressed in primitive variables, are always expressed in a Cartesian coordinate system, using a collocated arrangement. The large-eddy simulation (LES) technique is used in the simulations. For further information please see [18] [19].

The ALM has been implemented in the referred code [20]. In this model, the wind turbine rotor is represented as a body force field, where each blade is represented as a line that moves with the rotational speed of the rotor and it is discretized in radial sections where the aerodynamic forces are computed. To compute the force in each radial section, geometrical properties (chord length and twist angle) as well as aerodynamic properties (lift and drag coefficients) are determined. The latter are obtained from tabulated airfoil data. After computing the aerodynamic forces, it is required to project them from the representation of the rotor onto the computational domain. In order to compute the additional source term, a Gaussian smearing function with three coefficients, is used, taking into account the distance between each grid cell and radial section ( $d$ ), for each direction (n-normal direction, r-radial direction, t-tangential direction):

$$f(d) = \frac{1}{E_n E_r E_t \pi^{1.5}} e^{-\left(\frac{d_n}{E_n}\right)^2} e^{-\left(\frac{d_r}{E_r}\right)^2} e^{-\left(\frac{d_t}{E_t}\right)^2} \quad (1)$$

## 3. Validation case

### 3.1. Libertad wind farm

Libertad is a 7.7MW onshore wind farm, located in the south of Uruguay. It consists of four Vestas V100 wind turbine generators (WTG), two with rated power of 1.9MW (WTG1 and WTG2) and two of 1.95MW (WTG3 and WTG4), all four with a hub height of 95m and a rotor diameter of 100m. It has a meteorological mast with anemometers and wind vanes that measure wind speed and wind direction at 93m height. The wind farm location and layout are shown in Figure 1.



**Figure 1.** Libertad wind farm location (left) and layout (right)

### 3.2. Numerical setup

The size of the computational domain is 3.00km in the streamwise direction, 1.50km in the spanwise direction and 0.75km in the vertical direction. The domain is uniformly divided into 144 x 128 grid cells in the streamwise and spanwise directions respectively, while a stretched grid with 80 grid cells, is used in the vertical direction. The spatial resolution implies a resolution of R/2.4, R/4.3 in the streamwise and spanwise directions respectively, while in the vertical direction, 19 grid nodes cover the rotor diameter. A zero velocity gradient is imposed at the outlet and a wall model based on the log law is used to compute the stress at the surface while periodic conditions are used in the lateral boundaries. We use the Crank-Nicolson scheme to advance in time and the scale dependent dynamic Smagorinsky model to compute the subgrid scale stress [21][22]. The inflow condition is obtained from a precursor simulation. Figure 2 shows vertical profiles at the inlet boundary of the mean wind speed and turbulence intensity, averaged in the spanwise direction. At hub height the mean wind speed is 8.85m/s and the turbulence intensity 7.5%. Turbulence intensity is defined as the ratio between the standard deviation and the mean of the streamwise velocity.

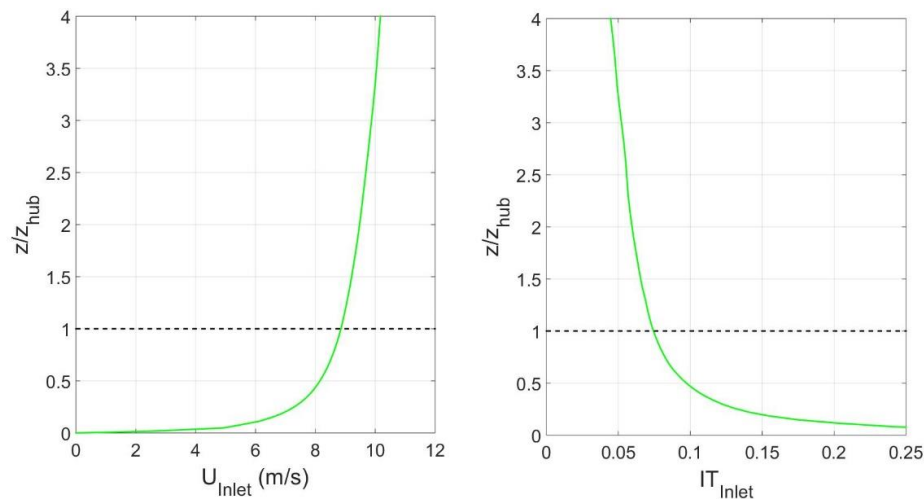


**Figure 2.** Mean wind speed (left) and turbulence intensity (right) vertical profiles at inlet boundary

To represent the wind turbine rotor, the ALM is used with 12 radial sections in each line. To find the chord length and twist angle in each radial section, the geometrical characteristics of the Vestas V80 wind turbine presented in [23], were modified according to the following methodology: We apply the Blade Element Momentum (BEM) model [24] with different wind speeds ( $U_{BEM}$ ), all of them lower

than the rated wind speed. For each  $U_{BEM}$  the SCADA data is sorted by  $U_{MET} \in [U_{BEM} \pm 0.25 \text{ m/s}]$ , where  $U_{MET}$  is the wind speed measured by the met mast anemometer. The blade rotating speed we use in BEM is the mean angular speed of the sorted dataset. The pitch angle is  $0^\circ$  in every case. Then, we compare the obtained power curve from BEM with the manufacturer's one and with the power curve obtained from the filtered SCADA data. We modify the geometrical characteristics of the blade and repeat the procedure until an acceptable agreement is obtained between the power curves. The airfoil used is the NACA 63-415 for the entire blade. Lift and drag coefficients were also obtained from [23]. The fact that the chord and twist angle obtained along the blades with this procedure are not the exact values of a V100 blade, contributes to the uncertainties of the results presented below. Figure 3 shows the designed chord length and twist angle, the power curve obtained from BEM compared with the SCADA data and the manufacturer's power curve (V100 PC), and the angular speed considered in BEM method.

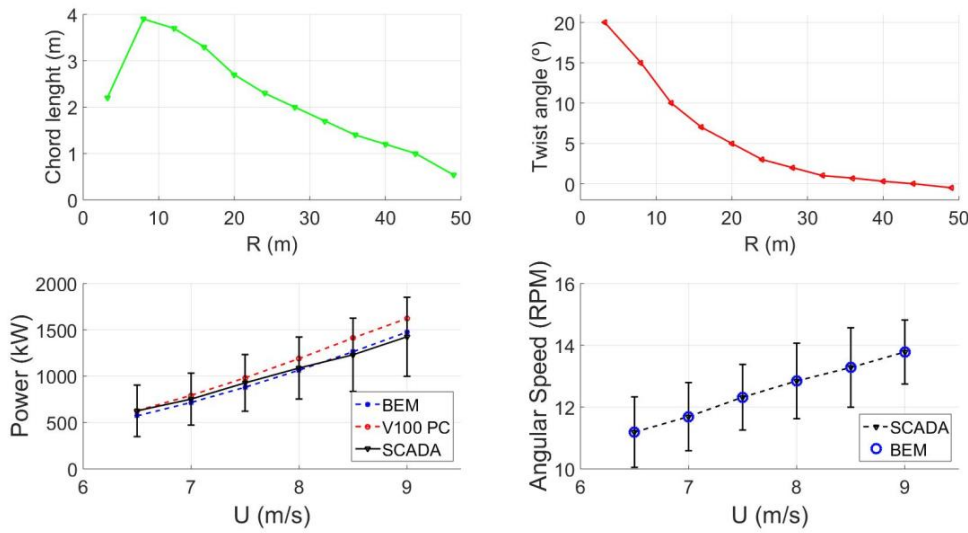


**Figure 3.** Designed chord length (top left), twist angle (top right), power curve (bottom left) and angular speed (bottom right) from BEM, SCADA data and manufacturer's power curve.

In the ALM implementation a variable rotational speed is considered, in a similar approach as explained in [23] for the Actuator Disk Model with Rotation, obtaining the relationship between the rotational speed of the rotor and its torque from the wind farm SCADA data. An efficiency of 0.93 is considered to compute the generated power from aerodynamic power [23].

#### 4. Results

Simulations considering different wind directions were performed by changing the layout while keeping the distance between wind turbines and the West boundary as inlet boundary [17]. Three wind sectors were considered,  $150 \pm 5^\circ$ ,  $150 \pm 2.5^\circ$  and  $132.5 \pm 2.5^\circ$ , as shown in Figure 1. In order to compute the power associated to each wind sector, weighted averages were computed taking into account the results of the simulations of different directions:

$$P_{av\ 150 \pm 5^\circ} = 12.5\% P_{145^\circ} + 25\% P_{147.5^\circ} + 25\% P_{150^\circ} + 25\% P_{152.5^\circ} + 12.5\% P_{155^\circ} \quad (2)$$

$$P_{av\ 150 \pm 2.5^\circ} = 25\% P_{147.5^\circ} + 50\% P_{150^\circ} + 25\% P_{152.5^\circ} \quad (3)$$

$$P_{av\ 132.5 \pm 2.5^\circ} = 25\% P_{130^\circ} + 50\% P_{132.5^\circ} + 25\% P_{135^\circ} \quad (4)$$

The power obtained in the simulations and the weighted averages were compared with the power registered in the SCADA data, which was filtered as follows. Only 10-minute periods which met the following criteria were considered:

- $U_{MET} \in [U_{MET\ sim} \pm 0.2\ m/s]$ , where  $U_{MET}$  is the wind speed registered by the met mast anemometer and  $U_{MET\ sim}$  is the mean wind speed obtained in the simulation at the met mast position
- $D_{MET} \in [D_{sim} \pm \Delta D^\circ]$ , where  $D_{MET}$  is the wind direction measured by the met mast wind vane,  $D_{sim}$  is the wind direction which is being simulated and  $\Delta D$  is the wind sector considered,  $5^\circ$  in the first case and  $2.5^\circ$  in the other two.
- The four wind turbines were available, their power was greater than zero and no alarms were reported.

No filtering was made in terms of turbulence intensity or atmospheric stability. The sorted data is represented as the mean power value  $\pm 1$  standard deviation.

When comparing the simulation results with SCADA datasets, the yaw misalignment of the turbines, the spatial variability of the wind direction within the wind farm and the variability of the wind direction within the averaging period, contribute to the uncertainties, as presented in [25].

The power simulation results and their average, are presented in Figure 4 and Figure 5, including also the SCADA data.

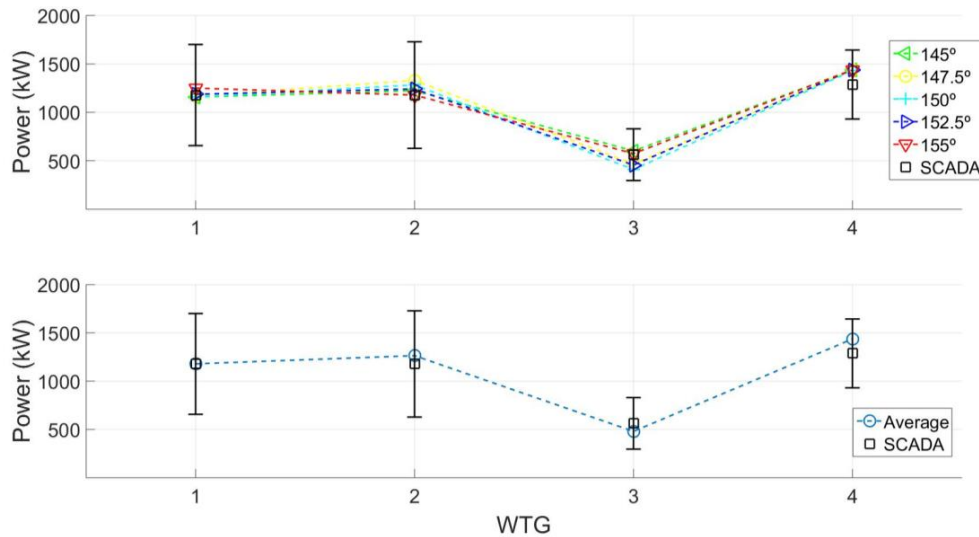


**Figure 4.** Power production of wind turbines for each direction ( $150\pm 5^\circ$ ) (top) and power weighted average by direction (bottom).

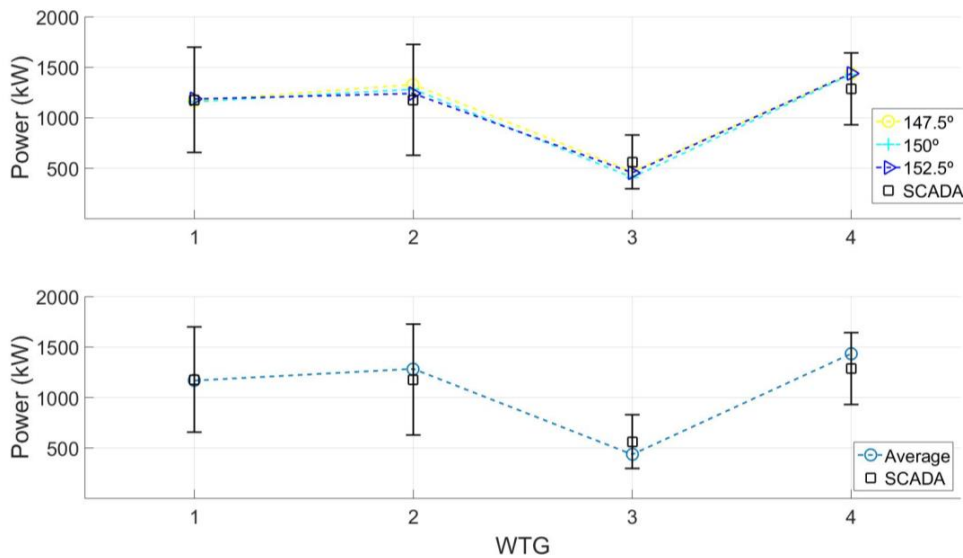


**Figure 5.** Power production of wind turbines for each direction (150+/-2.5°) (top) and power weighted average by direction (bottom)

The results show good agreement with the SCADA data in both cases, with no major differences between them, so a wind direction window of  $\pm 2.5^\circ$  was used when taking into account another wind sector below. The power deficit of WTG3 due to the wake of WTG4 is clearly shown in both figures, and it is slightly higher at 150° than in other directions, because the two wind turbines are aligned in that direction.

Another case was simulated, considering direction 132.5°, where WTG3, WTG2 and WTG1 are aligned. The mean wind speed at the met mast position is 8.89m/s. The results are depicted in Figure 6.

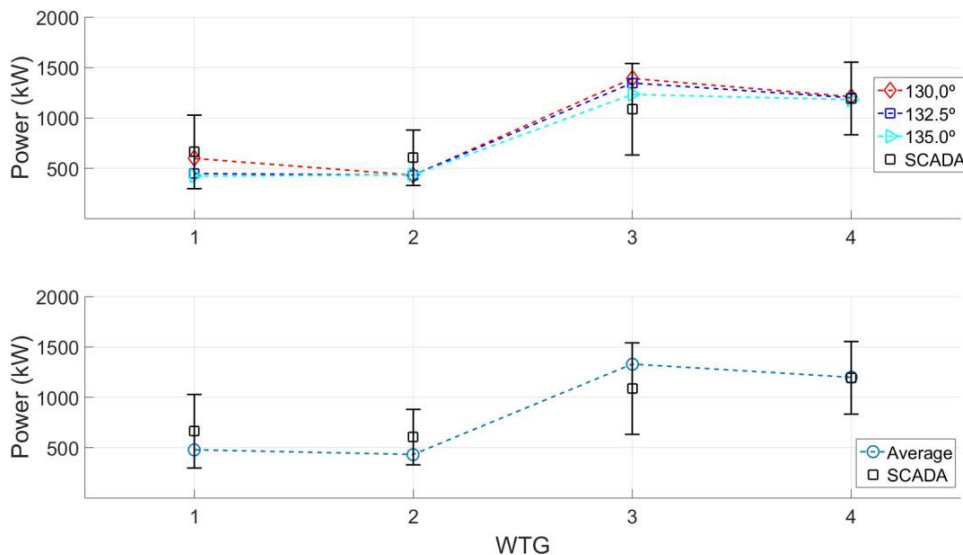


**Figure 6.** Power production of wind turbines for each direction (132.5+/-2.5°) (top), power weighted average by direction (bottom)

Results also show acceptable agreement with SCADA data, capturing WTG2 and WTG1 power deficits and overestimating WTG3 power production. An explanation of why this happens is presented below.

A simulation considering another inflow condition was performed, only for wind direction  $150^\circ$ . In this case, at the inlet and at hub height the mean wind speed is  $7.60\text{m/s}$  and the turbulence intensity is  $8.4\%$ . In Figure 7, the SCADA data is represented as scattered points, showing mean wind speed measured at the met tower and power production of the wind turbines, including the results of the simulations and also the manufacturer's power curve (V100 PC). The SCADA data is filtered by wind direction ( $150^\circ \pm 2.5^\circ$ ). Good agreement is observed for the four WTG. Notice how the SCADA scattered points of WTG3 are 'deviated' from the manufacturer power curve, due to the WTG4 wake.

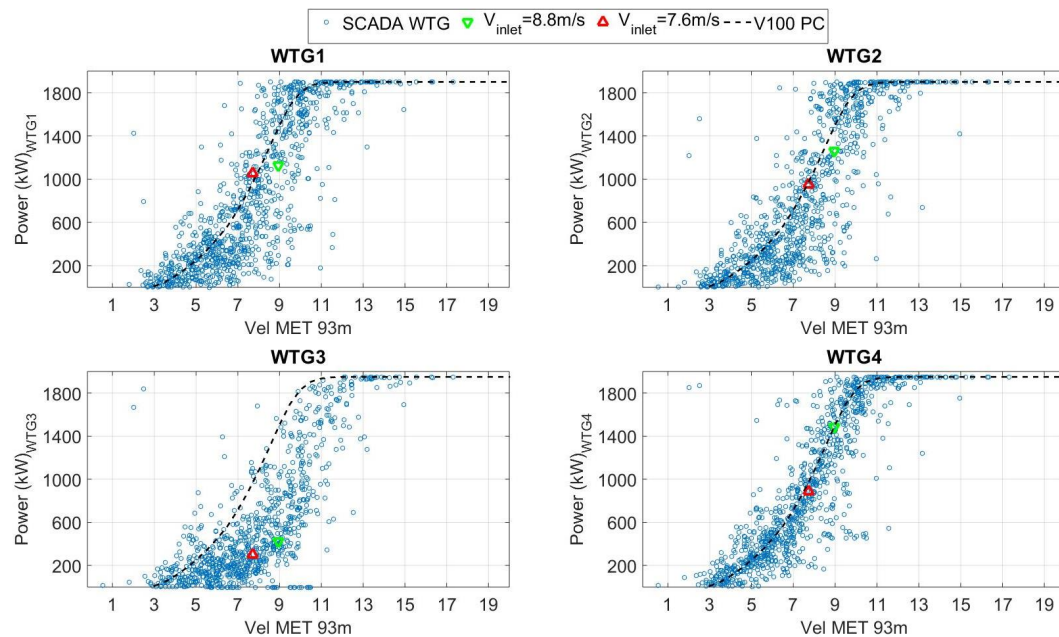


**Figure 7.** Simulated wind turbines mean power and scattered SCADA data filtered (wind direction  $150^\circ \pm 2.5^\circ$ ), for two inflow conditions.

The influence of the spatial resolution in the results was analyzed, by considering two more resolutions, which are R00 and R02, being R01 the original resolution. Their characteristics are presented in Table 1. As the length in the vertical direction is not uniform, only the height of the first cell is shown. NzD represents the number of cells which cover the WTG rotor in the vertical direction.

**Table 1.** Characteristics of resolutions

	Nx	Ny	Nz	$\Delta x(\text{m})$	$\Delta y(\text{m})$	$\Delta z_{\min}(\text{m})$	R/ $\Delta x$	R/ $\Delta y$	NzR
<b>R00</b>	192	144	96	15.6	10.4	2.5	3.2	4.8	23
<b>R01</b>	144	128	80	20.8	11.7	3.0	2.4	4.3	19
<b>R02</b>	128	96	72	23.4	15.6	3.0	2.1	3.2	17

Simulations considering wind direction  $150^\circ$  and mean velocity at the inlet and at hub height of  $8.8\text{m/s}$ , were performed. It is important to highlight that for each case a different precursor simulation was used, as the resolutions of the precursor simulations and the simulations with WTG must be the same. It is planned to implement the same precursor simulation for cases with different resolution in the near future. In Figure 8 the results for the three spatial resolutions are presented.

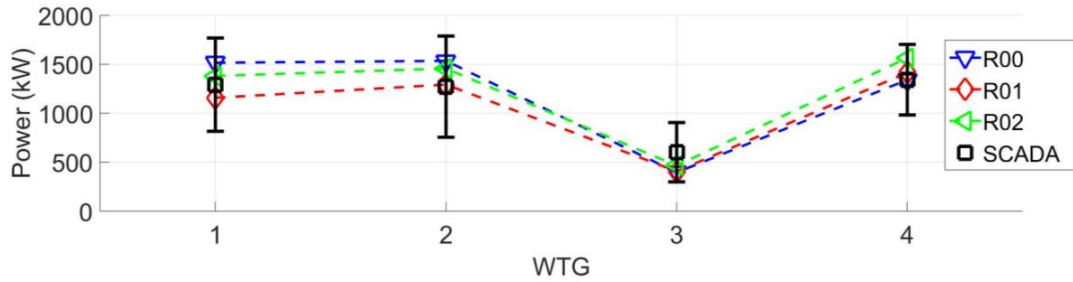


**Figure 8.** Power production of wind turbines considering three spatial resolutions, wind direction  $150^\circ$ . SCADA data filtered by wind direction:  $150^\circ \pm 2.5^\circ$ , wind speed  $8.91 \pm 0.2$  m/s.

Notice the dispersions in the results. For example, for R00 the power production of WTG4 is well predicted but the power production of WTG2 and WTG1 is overestimated, while in R01 the power production of WTG4 is slightly overpredicted and that of WTG1 is underpredicted. The reason for this is that as the precursor simulations are different, the velocity upstream the wind turbines is different in each case despite having almost the same velocity profile averaged in the spanwise direction. This is observed in Figure 9, where the mean streamwise velocity component ( $U$ ) is plotted, as vertical profiles at the inlet and at the met mast position. This figure also shows a surface plot of the streamwise velocity at the inlet section, with the WTG positions represented by the dotted circles, and the met mast position, by the smaller circle.

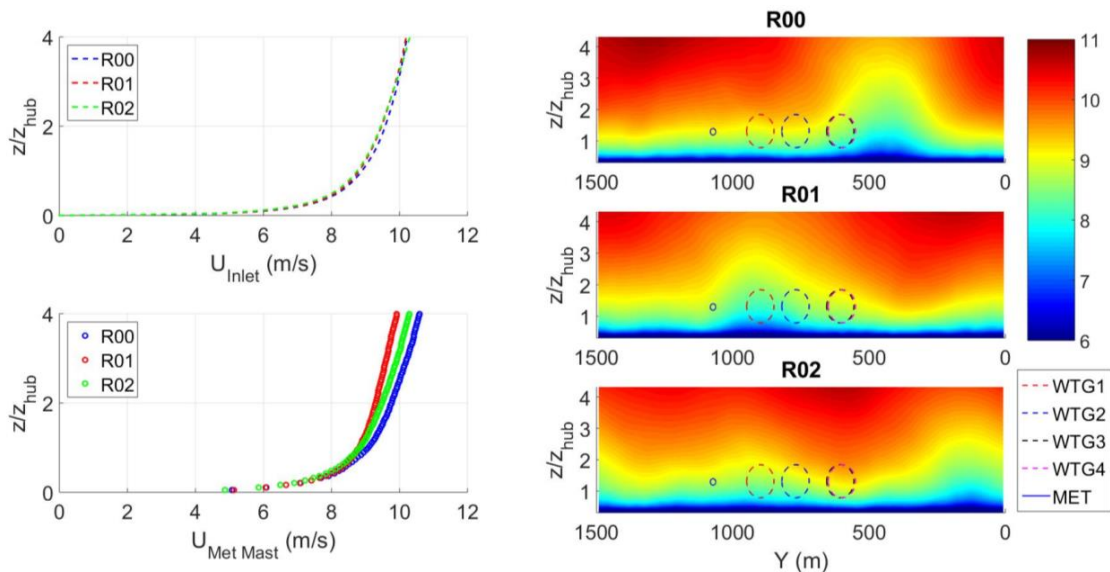


**Figure 9.** Vertical profiles of the mean streamwise velocity component ( $U$ ), averaged in the spanwise direction at the inlet (left above) and at the position of the meteorological mast (left bottom), and at the inlet section (right), for the three spatial resolutions considered.

Although the mean velocity averaged in the spanwise direction at the inlet is very similar for the three cases, notice how there are zones where the velocity is lower or higher than this value. When this zone is upstream of a WTG, the power production will be associated to this low/high velocity. For the same reason, it is also important to observe that at the position of the met mast the velocity may not represent the velocity averaged at the inlet, so when comparing the SCADA data of the wind turbines and the met mast data with the results of the simulations, this has to be taken into account. This explains why the power production of WTG2 and WTG1 are overestimated in R00, and why the power production of WTG1 is underestimated in the case of R01. This issue can also be observed in Figure 10, which shows the mean streamwise velocity ( $U$ ) in a horizontal plane at hub height, for the three resolutions.

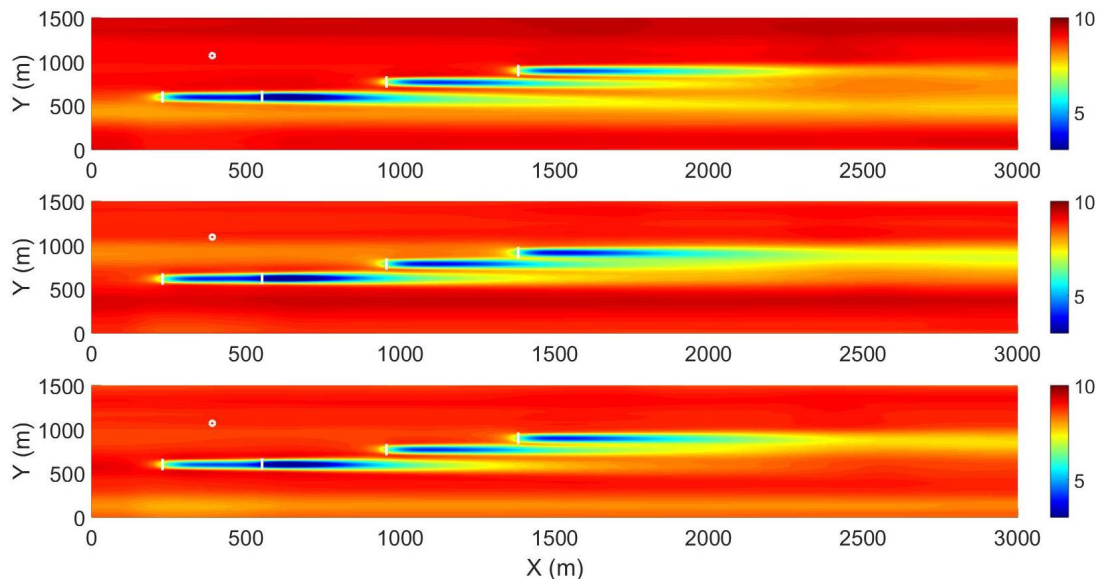


**Figure 10.** Mean streamwise velocity ( $U$ ), in a horizontal plane at hub height, for R00 (top), R01 (center) and R02 (bottom). White bars represent wind turbines, and white circle shows the position of the meteorological tower.

## 5. Summary and conclusions

The ALM has been validated under different conditions and used in different numerical codes, being one of the chosen approaches in the academic community, to represent the presence of wind turbines in a simulation. Expanding the work previously presented by the authors and to continue validating the capability of the numerical solver *caffa3d.MBRi* to simulate the flow through wind farms, the ‘Libertad’ onshore wind farm was simulated, representing the wind turbines with the ALM and with an atmospheric boundary layer like inflow condition.

Two different wind sectors ( $150^\circ$  and  $132.5^\circ$ ) with the same precursor simulation, and two precursor simulations with the same wind direction ( $150^\circ$ ) and different wind speed at hub height, were considered, in order to analyse the interactions and wakes of the wind turbines. Also for wind direction  $150^\circ$ , three spatial resolutions were considered. Good agreement with the SCADA data was found when assessing the power deficits observed in the data under those different conditions. When analysing the results with the three spatial resolutions, some differences were obtained. The causes may be related to the fact that the velocity at the position of the met mast may not be an accurate representation of the velocity at the inlet, as the velocity of the precursor simulation is not uniform in the spanwise direction, which leads to different velocities upstream of the positions of the wind turbines and the met mast.

Future research will be focused on the implementation of different control strategies to adjust the angular velocity of the rotor and the individual pitch of each blade, enabling to estimate power production at higher wind speeds and also assessing the operation of down-regulated wind farms. In addition to this, we plan to implement the same precursor simulation for different spatial resolutions, including mesoscale forcing, and to develop and evaluate wind farm control strategies, aiming to maximize the global power production of a wind farm.

## References

- [1] Global Wind Energy Council 2016 Global wind Report Annual Market Update 2015 (Brussels).
- [2] World Wind Energy Association 2014 Key statistics of world wind energy report 2013 (Shanghai).
- [3] International Energy Association 2013 Technology roadmap Wind Energy 2013 (Beijing).
- [4] Abkar M, Porté-Agel F 2013 The effect of free-atmosphere stratification on boundary-layer flow and power output from very large wind farms *Energies* **6** 2338-2361.

- [5] Lee S, Churchfield M, Moriarty P, Jonkman J, Michalakes J 2012 Atmospheric and Wake Turbulence Impacts on Wind Turbine Fatigue Loading *50th AIAA Aerospace Sciences Meeting* (Nashville, Tennessee).
- [6] Hansen K S, Barthelmie R J, Jensen L E, Sommer A 2012 The impact of turbulence intensity and atmospheric stability on power deficits due to wind turbine wakes at Horns Rev wind farm *Wind Energy* **15** 1 183-196.
- [7] Vanderwende B J, Lundquist J K 2012 The modification of wind turbine performance by statistically distinct atmospheric regimes *Environmental Research Letters* **7** 3 034035.
- [8] Sande B, van del Pijl S P and Koren B 2011 Review of computational fluid dynamics for wind turbine wake aerodynamics *Wind Energy* **14** 799-819.
- [9] Sørensen J N, Shen W Z 2002 Numerical modelling of wind turbine wakes *Journal of Fluids Engineering* **124** 2 393-99.
- [10] Troldborg N 2008 Actuator Line Modeling of Wind Turbine Wakes. PhD thesis, Technical University of Denmark.
- [11] Churchfield M J, Lee S, Moriarty P, Martínez L A, Leonardi S, Vijayakumar G and Brasseur J G 2012 A large-eddy simulation of wind-plant aerodynamics *50th AIAA Aerospace Sciences Meeting* (Nashville, Tennessee).
- [12] Porté-Agel F, Wu Y T, Lu H, Conzemius R J 2011 Large-eddy simulation of atmospheric boundary layer flow through wind turbines and wind farms *Journal of Wind Engineering and Industrial Aerodynamics* **99** (4) 154-168.
- [13] Troldborg N, Zahle F, Réthoré P E and Sorensen N N 2014 Comparison of wind turbine wake properties in non-sheared inflow predicted by different computational fluid dynamics rotor models *Wind Energy* doi: 10.1002/we.1757.
- [14] Pankjak K J, Churchfield M J, Moriarty P J and Schmitz S 2014 Guidelines for volume force distributions within actuator line modeling of wind turbines on large-eddy-simulation type grids *Journal of Solar Energy Engineering* **136** 031003-1-11
- [15] Draper M, Usera G 2015 Evaluation of the actuator line model with coarse resolutions *Wake Conference* (Visby).
- [16] Draper M, Guggeri A, Usera G 2016 Validation of the Actuator Line Model with coarse resolution in atmospheric sheared and turbulent inflow *Journal of Physics: Conference Series*, 753/8 (2016), 082007.
- [17] Draper M, Guggeri A, Usera G 2016 Modelling one row of Horns Rev wind farm with the Actuator Line Model with coarse resolution *Journal of Physics: Conference Series*, 753/8 (2016), 082028.
- [18] Usera G, Vernet A, Ferré J A 2008 A parallel block-structured finite volume method for flows in complex geometry with sliding interfaces *Flow, Turbulence and Combustion* **81** 471-495.
- [19] Mendina M, Draper M, Kelm Soares A P, Narancio G and Usera G 2014 A general purpose parallel block structured open source incompressible flow solver *Cluster Computing* **17** 2 231-41.
- [20] Draper M 2015 Simulación del campo de vientos y de la interacción entre aerogeneradores. PhD thesis (public defense July 2016), Universidad de la República.
- [21] Porté-Agel F, Meneveau C, Parlange M B 2000 A scale-dependent dynamic model for large-eddy simulation: application to a neutral atmospheric boundary layer *Journal of Fluid Mechanics* 415 261-284.
- [22] Stoll R, Porté-Agel F 2006 Dynamic subgrid-scale models for momentum and scalar fluxes in large-eddy simulations of neutrally stratified atmospheric boundary layers over heterogeneous terrain *Water Resources Research* 42 W01409.
- [23] Wu Y T, Porté-Agel F 2015 Modeling turbine wakes and power losses within a wind farm using LES: An application to the Horns Rev offshore wind farm *Renewable Energy* 75 945-55.
- [24] Hansen M 2008, Aerodynamics of Wind Turbines Second Edition, *Earthscand*.
- [25] Gaumont M, Réthore P-E, Ott S, Peña A, Bechmann A, Hansen K S 2014 Evaluation of the wind direction uncertainty and its impact on wake modeling at the Horns Rev offshore wind farm *Wind Energ.* **17** 1169-1178.

## **2.2. Paper 2: A High-Fidelity Numerical Framework For Wind Farm Simulations**

# A High-Fidelity Numerical Framework For Wind Farm Simulations

A. Guggeri\*, D. Slamovitz\*, M. Draper\* and G. Usera\*  
Corresponding author: aguggeri@fing.edu.uy

\* Facultad de Ingeniería, Universidad de la República,  
Julio Herrera y Ressig 565, Montevideo, Uruguay.

**Abstract:** A high fidelity numerical framework, based on a LES+ALM approach, to simulate the wind flow through wind farms is presented in this work. The operation of a 7.7MW onshore wind farm was simulated, considering different wind directions and subject to an atmospheric boundary layer (ABL) wind flow, and comparing the results with SCADA (Supervisory Control And Data Acquisition) data of the farm. Good agreement between the electric power and rotor speed mean values is found. Power and velocity deficits due to the wakes of the turbines were well captured in the simulations.

*Keywords:* Actuator Line Model, LES, Onshore Wind Farm.

## 1 Introduction

During the last decades, wind energy has seen big technological improvements, related to increases in hub height, rotor diameter and unit power, which has led to larger capacity factors for the same wind speed [1]. Those improvements have supported a rapid expansion all over the world, with annual growth rates of installed capacity around 20%. At present, horizontal axis wind turbines (HAWT) is the technology of greater installed capacity among renewable energies [2].

Recently it took place a significant development of methods and tools for performing high fidelity simulations of wind flows with presence of wind turbines applied to real wind farms. Methods in the frame of Reynolds Averaged Navier-Stokes (RANS) or Large Eddy Simulations (LES) for resolving the wind flow, alongside the Actuator Line Model (ALM) for representing the wind turbines rotors, in which those are represented as body forces. Generally, the strategy followed for simulating a real wind farm under different wind conditions, particularly under different wind directions, has been LES-ADM-R [3] [4], while LES-ALM based methods have been used for evaluating specific wind conditions, particularly one specific wind direction [5] [6] [7]. Based on the precedent, this paper presents an application of the LES-ALM methodology, used for simulating a real wind farm under various wind conditions.

The aim of the present paper is to validate a tool for simulating the operation of a wind farm for numerous wind directions. With that purpose, simulations of the onshore wind farm 'Libertad' were performed. The wind farm consists of 4 wind turbines, Vestas v100, having 2 of them a nominal power of 1950 kW and the remaining 2 a nominal power of 1900 kW. An atmospheric boundary layer (ABL) like inflow condition is considered, along with 14 wind directions, within which, some show strong interactions between the turbines due to their wakes. The *caffa3d.MBRI* solver is used to simulate the wind flow, and the Actuator Line Model (ALM) is used to represent the turbines. The results obtained from the simulations seem acceptable when compared with SCADA data.

The rest of the paper is organized as follows: Section 2 presents a brief description of the numerical solver *caffa3d.MBRI* and the implementation of the ALM, Section 3 describes the wind farm mentioned above, Section 4 describes the simulation setup, Section 5 presents the main results, and conclusions are given in Section 6.

## 2 Numerical Model

### 2.1 CFD solver

caffa3d.MBRi [8] [9] is an open source, finite volume (FV) code, second order accurate in space and time, parallelized with MPI, in which the domain is divided in unstructured blocks of structured grids. The mathematical model comprises the mass balance equation (1) and momentum balance equation (2) for a viscous incompressible fluid, together with generic passive scalar transport equation (3) for scalar field  $\phi$  with diffusion coefficient  $\Gamma$ . Note that (2) has been written only for the first Cartesian direction  $\hat{e}_1$ . The balance equations are written for a region  $\Omega$ , limited by a closed surface  $S$ , with outward pointing normal  $\hat{n}_S$ .

$$\int_S (\vec{v} \cdot \hat{n}_S) dS = 0 \quad (1)$$

$$\int_{\Omega} \rho \frac{\partial u}{\partial t} d\Omega + \int_S \rho u (\vec{v} \cdot \hat{n}_S) dS = \int_{\Omega} \rho \beta (T - T_{ref}) \vec{g} \cdot \hat{e}_1 d\Omega + \int_S -p \hat{n}_S \cdot \hat{e}_1 dS + \int_S (2\mu D \cdot \hat{n}_S) \cdot \hat{e}_1 dS \quad (2)$$

$$\int_{\Omega} \rho \frac{\partial \phi}{\partial t} d\Omega + \int_S \rho \phi (\vec{v} \cdot \hat{n}_S) dS = \int_S \Gamma (\nabla \phi \cdot \hat{n}_S) dS \quad (3)$$

where  $\vec{v} = (u, v, w)$  is the fluid velocity,  $\rho$  is the density,  $\beta$  is the thermal expansion factor,  $T$  is the fluid temperature and  $T_{ref}$  a reference temperature,  $\vec{g}$  is the gravity,  $p$  is the pressure,  $\mu$  is the dynamic viscosity of the fluid and  $D$  is the strain tensor. The use of equations in their global balance form, together with the finite volume method, as opposed to the differential form, favors enforcing conservation properties for fundamental magnitudes as mass and momentum into the solving procedure [10].

Representation of complex geometries can be handled through a combination of body fitted grids and the immersed boundary method over both Cartesian and body fitted grid blocks. Geometrical properties and flow properties, which are expressed in primitive variables, are always expressed in a Cartesian coordinate system, using a collocated arrangement. Regarding the turbulence model, different subgrid scale models in the context of Large Eddy Simulation (LES) are implemented: the standard Smagorinsky model [11] with damping function for smooth [10] and rough surfaces [12], the dynamic Smagorinsky model [13] with different averaging schemes, the dynamic mixed Smagorinsky model [14] and the scale-dependent dynamic Smagorinsky model [15] with different averaging schemes. Further details of the solver together with validations can be found in [8, 16].

### 2.2 Actuator Line Model

The ALM has been implemented in the code [17] to represent wind turbines rotors in the simulations.

Each blade is represented as a line that moves with the rotational speed of the rotor and is discretized in radial sections where the aerodynamic forces are computed (Figure 1, left). The geometrical properties of the blades (chord length and twist angle ( $\beta$ )) as well as aerodynamic properties (lift and drag coefficients) are necessary to compute the force in each radial section (Figure 1, right). The former are obtained directly from the wind turbine model, while the aerodynamic coefficients are computed from tabulated data of the corresponding airfoil. At each radial section the aerodynamic force is computed as equation 4.

$$\vec{f} = -\frac{1}{2} \rho V_{rel}^2 c (C_L \vec{e}_L + C_D \vec{e}_D) dr \quad (4)$$

where  $\rho$  is the air density,  $V_{rel}$  is the relative velocity,  $c$  is the chord length,  $C_L$  is the lift coefficient,  $C_D$  is the drag coefficient,  $\vec{e}_L$  is a unit vector in the direction of the lift force,  $\vec{e}_D$  is a unit vector in the direction of the drag force and  $dr$  is the length of the radial section. Prandtl's tip loss correction factor is applied, as it has shown to improve the results [18].

After computing the aerodynamic forces, it is required to project them onto the computational domain as a body force field. To accomplish this, a smearing Gaussian function is used, taking into account the

distance between each grid cell and radial section, and three smearing parameters, one for each direction ( $n$  normal,  $r$  radial and  $t$  tangential).

$$f(d_n, d_r, d_t) = \frac{1}{\epsilon_n \epsilon_r \epsilon_t \pi^{1.5}} e^{-\left(\frac{d_n}{\epsilon_n}\right)^2} e^{-\left(\frac{d_r}{\epsilon_r}\right)^2} e^{-\left(\frac{d_t}{\epsilon_t}\right)^2} \quad (5)$$

At each time step of the simulation, the resulting aerodynamic torque applied to the rotor shaft ( $M_{aero}$ ) is computed by integration of the tangential forces along the blades, and the rotational speed is obtained from the rotor second cardinal equation (6).

$$I \frac{d\omega}{dt} = M_{aero} - M_{gen} \Rightarrow \omega = \frac{(M_{aero} - M_{gen})}{I} \Delta t + \omega_{t-1} \quad (6)$$

where  $M_{gen}$  is the generator torque,  $\omega$  is the angular speed of the rotor at the current time step,  $I$  is the sum of the rotor, shaft and generator inertia considered at the low-speed side.  $\Delta t$  corresponds to the temporal step and  $\omega_{t-1}$  accounts for the rotational speed of the previous time step. Finally, the aerodynamic and electric power are calculated as the rotational speed multiplied by the shaft aerodynamic torque and the generator torque, respectively (Eq. 7).

$$P_{aero} = M_{aero} \cdot \omega \quad (7)$$

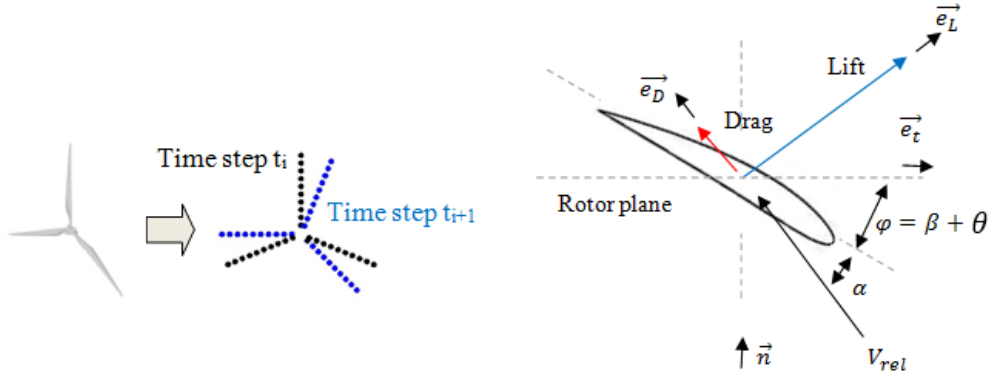


Figure 1: ALM rotor representation (left) and a cross-sectional airfoil radial section (right).

### 3 Validation case

The simulated wind farm, Libertad, is the same as described in [4]: it is a 7.7MW onshore wind farm located in the south of Uruguay, which has been operating since August 2014 by the Uruguayan company Ventus. It consists of four Vestas V100 wind turbine generators (WT), two with rated power of 1.9MW (WT1 and WT2) and two of 1.95MW (WT3 and WT4), all four with a hub height of 95m and a rotor diameter of 100m. The farm has a meteorological mast (MM) with anemometers at 95m, 80m and 60m, and wind vanes at 93m and 58m height. The wind farm location and layout are shown in Figures 2 and 3.

The terrain surrounding the wind turbines is plane, with no significant slopes according to annex B of IEC 61400-12-1 Standard. Figure 4 shows the wind frequency rose, considering the whole period of operation of the wind farm, almost 4 years, where a predominance of winds coming from the northeast can be observed, which is consistent with the wind farm layout design (see Figure 3).

The data acquired by the SCADA system of the turbines and from the meteorological instruments is compared with the simulations results. The wind turbines data is acquired on a 1 Hz frequency, and recorded on a 10-minute basis, where the mean, standard deviation, maximum and minimum values of more than 250 SCADA signals are available. For this work we consider the 10-minute average of the following 7 signals



Figure 2: Wind farm location



Figure 3: Wind farm layout

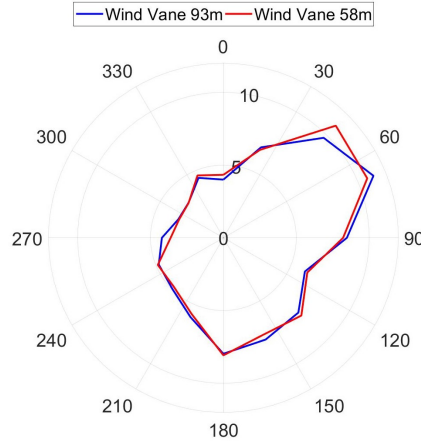


Figure 4: Wind frequency rose

of each turbine: electric power, wind speed, rotor angular speed, blades pitch angle, turbine availability, alarm-code, and active power reference; and from the meteorological instruments, at each mentioned height, we consider the mean values of wind velocity and direction. Table 1 depicts the signals, their source of measurement, symbols and unity. Sub-index  $i = 1 : 4$  refers to each wind turbine; sub-index  $j = 95, 80, 60$  refers to mast anemometers heights; sub-index  $h = 93, 58$  refers to mast wind vane heights. The velocity standard deviation ( $\sigma(U)$ ) is used to compute the turbulence intensity according to equation 8.

$$TI = \sigma(U)/\bar{U} \quad (8)$$

To compare with the simulation results, only the 10-minute periods with normal operation of the wind turbines is taken into account, so the data is filtered according to the following criteria:

- $AA = 0$
- $OK > 595s$
- $P_{Ref} = P_{rated}$
- $\theta < 90^\circ$

Table 1: Signals of WT SCADA and MM instruments

Signal	Source	Symbol	Unity
Electric power	$WT_i$	$P$	$kW$
Wind velocity	$WT_i$	$V_{WT}$	$m/s$
Rotor Angular Speed	$WT_i$	$\Omega$	$RPM$
Blade pitch angle	$WT_i$	$\theta$	$^\circ$
Turbine availability	$WT_i$	$OK$	$s$
Alarm-code	$WT_i$	$AA$	non dimensional
Active power reference	$WT_i$	$P_{Ref}$	$kW$
Wind velocity	$MM_{Height_j}$	$V_{MMH_j}$	$m/s$
Wind turbulence intensity	$MM_{Height_j}$	$TI_{MMH_j}$	$\%$
Wind direction	$MM_{Height_k}$	$d_{MMH_k}$	$^\circ$

Considering the filtered data, Figure 5 depicts a scatter plot of velocity vs power measured at the turbine, together with the manufacturer power curve, for each WT. Still after applying the mentioned filters, a high dispersion of the data can be observed, which can be explained by the following reasons, among others: the natural temporal and spacial variability of the wind, particularly for each direction there is a different terrain influence and turbine-wake interaction; the atmospheric stability, with different wind shear profiles and turbulence intensities, which affect the operation of the WT as well as the characteristics of their wakes; and also other operational aspects of the turbines, such as degradation of their components over time, for example the blades, also contribute to the dispersion of the scatter.

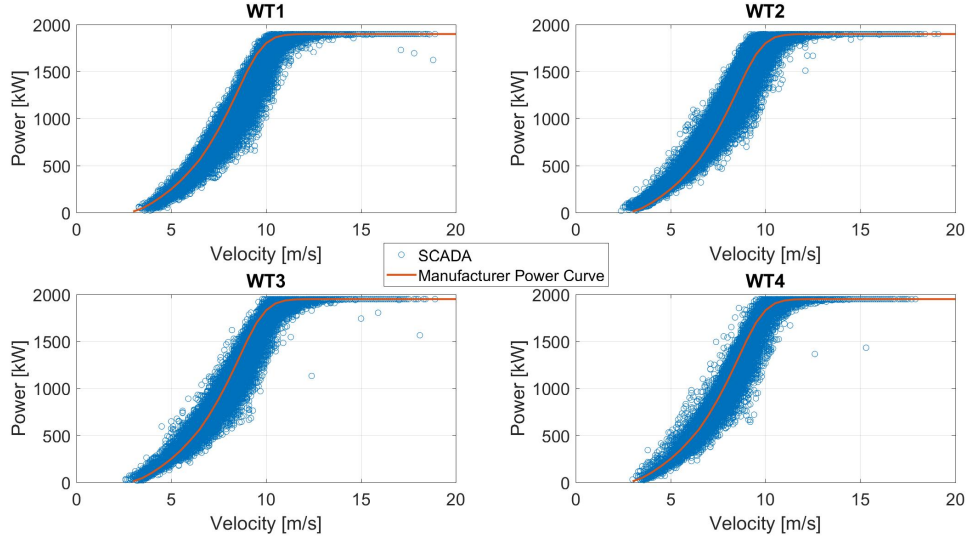


Figure 5: Scatter plot of SCADA velocity vs power manufacturer power curve

For the comparison with the simulation results, additional filters are applied to the SCADA dataset, considering the wind direction measured by the wind vane at 93m, and wind velocity measured by the anemometers at 95m, according to the following criteria:

- $V_{MM95} \in (V_{Ref} \pm 0.25m/s)$
- $d_{MM93} \in (D_{Ref} \pm \Delta d ^\circ)$

Where  $V_{Ref}$  correspond to the wind velocity of the simulation at hub height (95m) and 280 meters upstream of the first WT of on the row. The reason to consider this value rather than the velocity at a fixed position, for example at the meteorological mast is the span-wise variability of the velocity at the inlet, and is further explained in Section 4.2.

$(D_{Ref} \pm \Delta d ^\circ)$  represents a wind sector:  $D_{Ref}$  accounts for the average of two consecutive simulations while  $\Delta d$  is the difference between  $D_{Ref}$  and the direction of an individual simulation, in some cases  $5^\circ$  and in others  $10^\circ$ . For example, for simulations  $150^\circ$  and  $160^\circ$ ,  $D_{Ref}$  is  $155^\circ$  and  $\Delta d = 5^\circ$ ; for simulations  $200^\circ$  and  $220^\circ$ ,  $D_{Ref}$  is  $210^\circ$  and  $\Delta d = 10^\circ$ . In order to compute the power and rotor speed associated to each wind sector, averages were computed taking into account the results of the consecutive simulations. No filters considering turbulence intensity or wind shear were applied, as in that case too few data would have fulfilled the criteria. As explained previously in this Section, these atmospheric variables contribute to the dispersion of the power values, as it will be noticed on Section 5. Results.

## 4 Simulation setup

This Section is divided into three subsections. The first one details the characteristics of the domain, grid, time step, boundary conditions, and wind turbines representation; the second presents the precursor simulation used as inlet boundary condition of the simulations; and the third Subsection describes the axiomatization of the procedure for simulating the operation of the wind farm for numerous wind directions.

### 4.1 Numerical setup

The size of the computational domain for all the simulations is 3.60km x 1.80 km x 0.75 km, the domain is uniformly divided into 288 and 256 cells in the stream-wise and span-wise directions respectively, while in the vertical direction it is divided in 96 cells, which grow up with the distance to the floor with an expansion coefficient of 1.0178. The domain is divided in 16 blocks, which are used for the parallelization with MPI. The inflow condition is obtained from a precursor simulation, while zero velocity gradient is imposed at the outlet and a wall model based on the log law is used to compute the stress at the surface. Periodic conditions are used in the lateral boundaries, and symmetry at the top. The spatial resolution implies a resolution close to R/4.0, R/7.1, R/6.5 in the stream-wise, span-wise and vertical directions respectively; in the vertical direction 23 grid nodes cover the rotor diameter. This grid configuration is the very similar to the thinnest one used in [4]

The Crank-Nicolson scheme is used to advance in time and the scale dependent dynamic Smagorinsky model to compute the subgrid scale stress. To represent the wind turbine rotor the ALM is used the same manner as [4]. The presence of the tower and nacelle are taken into account through drag coefficients, in a similar approach as presented in [19]. The chord and twist angles as well as the airfoil's data, and the relationship between the rotational speed of the rotor and its torque are taken from [4]. Considering the angular velocity of the rotor, the spacial resolution, and previous experiences [4], the temporal step is set at 0.20s.

### 4.2 Precursor simulation

The precursor simulates an ABL like wind flow, in a domain of the same size and using the same resolution than the domain used for the main simulations, but without considering the topography nor the wind turbines. It is generated considering periodic boundary conditions, with a constant pressure gradient as forcing term, and runs until it reaches statistical convergence. The time evolution of a transversal plane of the precursor is considered as boundary condition at the entrance of the main simulations, as it is usually done for this type of simulations [20] [21] [4].

Figure 6 shows the stream-wise velocity component at the inlet of the simulations, where a significant variation along the span-wise direction can be noticed. This problem has already been observed by the

authors of this paper [4], while in [22] the strategy proposed in [23] is applied to simulate a neutral atmospheric turbulent boundary layer flow with a single turbine and an aligned wind farm, and compared them with a well known experimental campaign. The issue with this span-wise variation is that the velocity at a fixed position of the simulation domain, for example the position of the meteorological mast, may not be representative of the velocity of the whole wind farm when different wind directions are simulated. For this reason, in this work, we consider the reference velocity ( $V_{Ref}$ ) as the wind velocity of the simulation at hub height (95m) and 280 meters upstream of the first WT of the row. For wind directions between  $60^\circ$  and  $240^\circ$  it is WT4 and for the rest of directions it is WT1. This ( $V_{Ref}$ ) is used to filter the SCADA data as described in Section 3. It is planned to implement a similar strategy to the one proposed in [23] in the near future, to avoid having a significant span-wise velocity variation at the inlets.

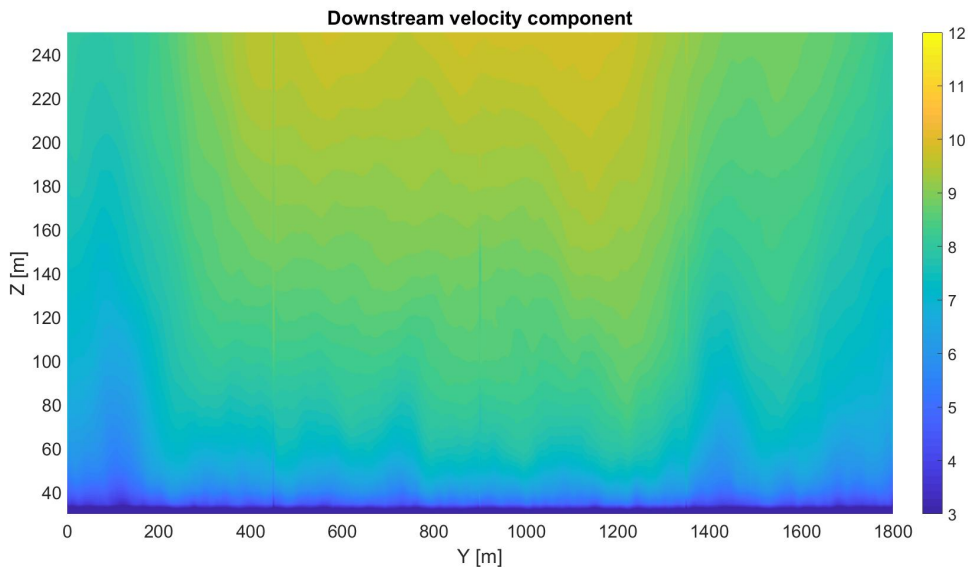


Figure 6: Stream-wise velocity component at the inlet of the simulations

### 4.3 Automatic grid creation and simulation setup

For simulating numerous directions, the procedure has been automatized, with a Matlab script that has been written and run for this purpose. Some of the inputs for this scripts are the coordinates of the wind turbines and meteorological masts, the height curves around them (e.g in a Computer-Aided Design (CAD) file), the directions aimed to be simulated, alongside other inputs with details of the domain, grid and temporal resolution, wind turbines model, boundary conditions, and computational requisites for the simulation to be run in the computer-cluster. For each direction, the script rotates the domain for making the inlet plane coincide with the west face of the domain. Then it crops the domain according to the given wind direction, domain size and resolution, and it generates all the necessary input files for generating the simulation grid, taking into account the topography and the turbines positions. Those input files are sent to the computer-cluster of Facultad de Ingeniería, where the grid is generated, the simulation is set-up and then begins running, all in an automatic manner. For the wind farm presented in this paper, the procedure until this step takes around 35 minutes, in a 3.6 GHz processor, for each wind direction.

For this wind farm, each simulation requires 16 cores of the cluster (64 GB RAM, Intel(R) Xeon(R) CPU E5-2650 @ 2.00GHz), one for each block. 4000 temporal steps are run, which takes approximately 80 hours, discarding the first 1000 in order to avoid unwanted transitory phenomenons due to sudden appearance of the turbine in the simulations. 3000 temporal steps remain then, which equals to 10 minutes and accounts for 150 turns of the rotor.

Figure 7 illustrates the rotation and cropping of the domain, for direction  $150^\circ$ . At the top left it shows the topography of the domain around the wind farm, with the wind farm location indicated with a red square, at top right it depicts the topography rotated for simulating wind coming from  $150^\circ$  (measured clockwise from the North); then at the bottom the domain used for simulating that direction is shown, where the wind farm topography as well and the wind turbines and meteorological mast positions are shown in better detail.

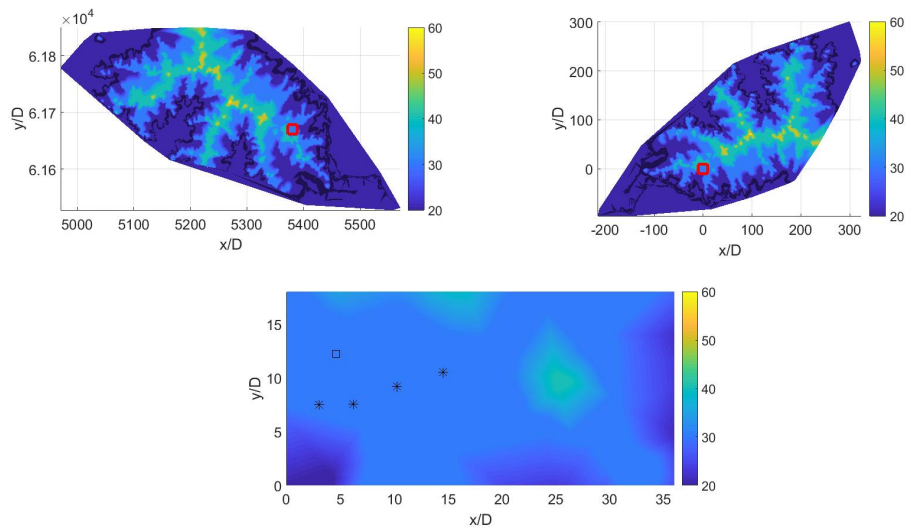


Figure 7: Original domain topography, with the wind farm zone marked in red (up and left),  $150^\circ$  rotated domain topography, with the wind farm zone marked in red (up and right), and  $150^\circ$  rotated and cropped domain topography, with the wind turbines marked with crosses and the meteorological mast marked with a square (down)

## 5 Results

In this section the results of the wind farm simulations for 14 different wind directions are presented, as described in Section 4, and compared with the data presented in Section 3.

Table 2 depicts the mean values of power and rotor speed, discriminated by wind sector, for each wind turbine and total mean power for the entire farm. The SCADA data is presented as the mean value of datums that fulfill the filters criteria,  $\pm$  the standard deviation of those datums. Notice that the standard deviation takes values of the order of hundreds of kW, which is consistent with what is observed in Figure 5. The relative difference between the simulation and SCADA data as well as the standard deviation of the SCADA datasets are also presented. Although significant differences can be observed in some cases, the highest being 57% for WT3 at wind sector  $325 \pm 5^\circ$ , in all the other cases the simulation averaged value lies between  $\pm 1$  standard deviation of SCADA data, both for power and rotor speed. In part, this is due to the high variability of the SCADA data, and because the simulations represent just a particular case among them.

Wind Turbine	Wind sector	D	125	135	145	155	170	190	210	230	305	315	325	335
		DeltaD	5	5	5	5	10	10	10	10	5	5	5	5
WT1	Power [kW]	Simulation	1007	847	1289	1531	1509	1272	1127	1167	1473	1455	1441	1440
		SCADA	1080	840	1063	1368	1374	1619	1298	1363	1180	1144	1471	1624
		SCADA Std	350.1	400.7	423.1	313.2	285.8	305.3	353.1	343.9	325.9	477.8	375.3	318.7
	Rotor Speed [RPM]	Simulation	12.8	12.4	14.0	14.5	14.5	14.0	13.6	13.7	14.4	14.4	14.4	14.4
		SCADA	13.4	12.4	13.1	14.2	14.2	14.5	14.0	14.2	14.1	13.9	14.5	14.7
		SCADA Std	1.08	1.26	1.28	0.78	0.69	0.67	0.97	0.76	0.84	0.85	0.75	0.50
Difference		-4%	0%	6%	2%	2%	-4%	-3%	-3%	2%	3%	0%	-2%	
Difference		-7%	1%	21%	12%	10%	-21%	-13%	-14%	25%	27%	-2%	-11%	
WT2	Power [kW]	Simulation	708	635	1146	1519	1528	1516	1497	1500	1025	769	1197	1467
		SCADA	907	814	1043	1411	1489	1588	1349	1380	1163	820	1130	1648
		SCADA Std	374.6	366.7	427.0	335.8	257.0	296.6	291.3	304.9	353.8	451.9	404.2	332.7
	Rotor Speed [RPM]	Simulation	11.8	11.5	13.4	14.5	14.5	14.5	14.5	14.5	12.9	12.1	13.6	14.5
		SCADA	12.5	11.9	12.7	13.9	14.3	14.3	13.7	13.9	13.5	11.8	12.7	14.5
		SCADA Std	1.18	1.19	1.26	0.94	0.64	0.77	0.93	0.79	1.02	1.85	1.48	0.73
Difference		-6%	-3%	6%	5%	2%	2%	6%	4%	-5%	2%	7%	0%	
Difference		-22%	-22%	10%	8%	3%	-5%	11%	9%	-12%	-6%	6%	-11%	
WT3	Power [kW]	Simulation	1507	1139	567	703	1280	1479	1468	1478	835	1001	1453	1499
		SCADA	1264	1203	788	727	1183	1500	1227	1307	775	636	1178	1604
		SCADA Std	295.9	358.6	378.6	357.5	347.0	327.3	334.5	304.1	372.6	289.0	463.1	349.7
	Rotor Speed [RPM]	Simulation	14.5	13.4	11.0	11.6	13.9	14.5	14.5	14.5	12.4	12.8	14.4	14.5
		SCADA	14.0	13.6	12.2	11.8	13.5	14.2	13.6	14.0	12.3	11.2	13.1	14.5
		SCADA Std	0.92	1.04	1.37	1.24	0.98	0.78	1.01	0.74	1.25	1.34	1.55	0.79
Difference		4%	-2%	-10%	-2%	3%	2%	6%	4%	0%	14%	10%	0%	
Difference		19%	-5%	-28%	-3%	8%	-1%	20%	13%	8%	57%	23%	-7%	
WT4	Power [kW]	Simulation	1489	1483	1443	1432	1435	1386	1361	1389	1377	939	476	750
		SCADA	1259	1377	1346	1336	1338	1505	1247	1330	1229	860	622	1148
		SCADA Std	284.4	276.1	306.2	294.8	289.2	329.9	340.4	321.9	383.4	493.8	314.6	705.8
	Rotor Speed [RPM]	Simulation	14.4	14.4	14.4	14.4	14.4	14.3	14.3	14.3	14.3	12.7	10.7	11.7
		SCADA	13.8	14.0	13.8	13.8	13.8	14.0	13.5	13.7	13.8	12.1	11.4	12.7
		SCADA Std	0.83	0.74	0.91	0.75	0.76	0.83	1.02	0.80	1.04	1.86	1.24	2.24
Difference		5%	3%	4%	4%	4%	2%	6%	4%	3%	4%	-6%	-8%	
Difference		18%	8%	7%	7%	7%	-8%	9%	4%	12%	9%	-24%	-35%	
Wind Farm	Power [kW]	Simulation	4711	4104	4445	5186	5751	5652	5452	5534	4710	4164	4566	5155
		SCADA	4510	4234	4240	4842	5385	6212	5120	5380	4348	3459	4402	6023
		SCADA Std	1108	1149	1204	1116	1052	1141	1196	1146	1250	1532	1232	1592
		Difference	4%	-3%	5%	7%	7%	-9%	6%	3%	8%	20%	4%	-14%

Table 2: Simulation and SCADA mean power and rotor speed values, by wind sectors

Figure 8 depicts the mean power by wind sector for each wind turbine, considering the data shown in Table 2 and also the results of the individual simulations, from where the averages were computed. Higher differences can be observed with the individual simulation results rather than the averaged values, as it was expected, as they represent the operation of the wind turbine at particular wind direction, rather than a wind sector. Power deficits can be clearly noticed for each wind turbine, consistent with the layout shown in Figure 3

Figure 9 shows the whole wind farm power output. In this case the power deficits at sectors  $[130^\circ \ 150^\circ]$  are still present, although less significantly, as the rest of the turbines compensate the power deficit of a particular one.

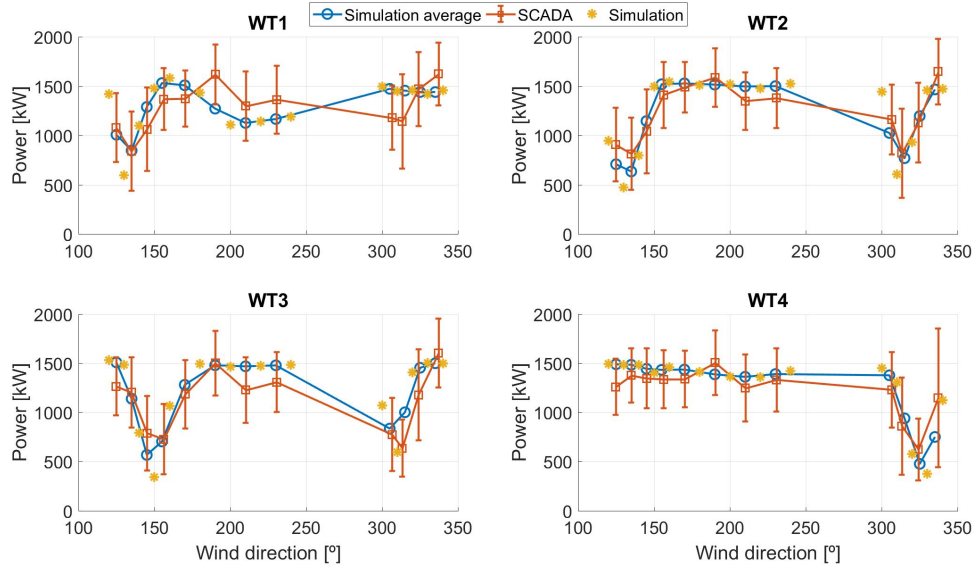


Figure 8: Mean power by direction, simulations vs SCADA data for each wind turbine

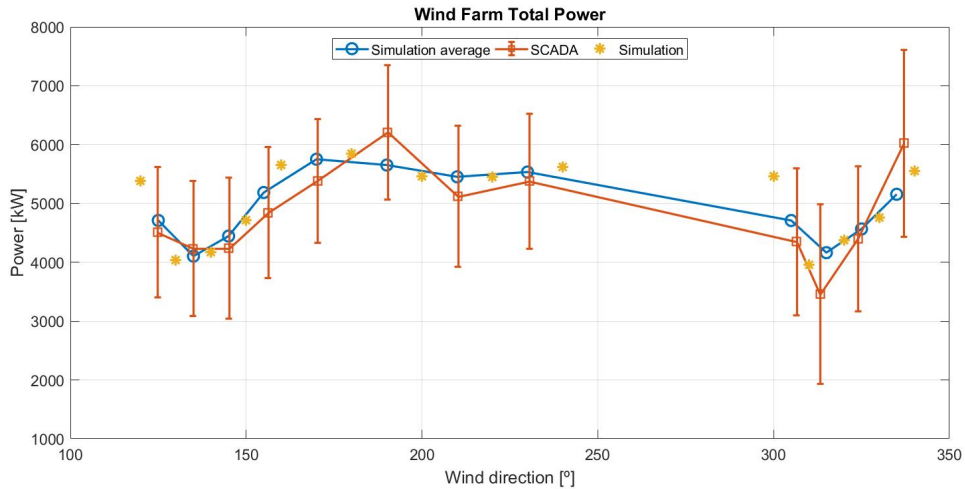


Figure 9: Mean power by direction, simulations vs SCADA data for the whole wind farm

Figure 10 depicts the mean stream-wise velocity on a horizontal plane at hub height, for two directions:  $150^\circ$  and  $180^\circ$ . The wakes downstream the rotors can be clearly identified, characterized by a large velocity deficit extending beyond  $10D$  downstream. While for the  $180^\circ$  direction, each wind turbine operates without the influence of another WT wake; at  $150^\circ$  the second wind turbine in the row (WT3) is just downstream of WT4, causing its power deficit, as can be seen in Figure 8.

Figure 11 shows the rotor speed of the four WT. Good agreement is found between simulations and SCADA data. When the turbines operate at below rated wind speed, the rotational speed is strongly related to the velocity upstream of the turbine, as it is regulated to operate at the optimal tip speed ratio (TSR) and thus extract the maximum possible power from the wind [24].

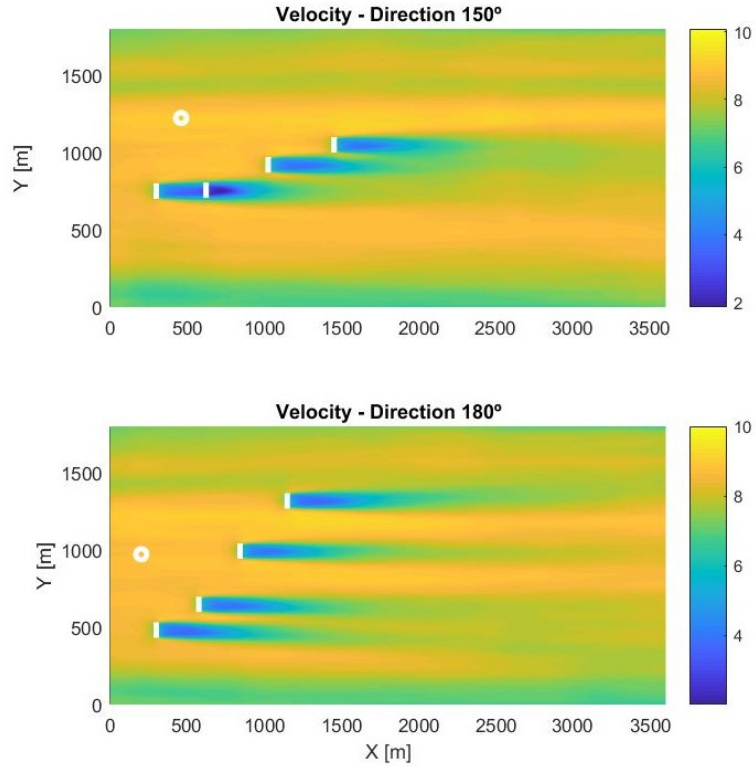


Figure 10: Mean stream-wise velocity, on horizontal plane at hub height, for two directions: Top: 150 ° ; Bottom: 180 ° Wind turbines are represented by white line, and the mast by the white circle

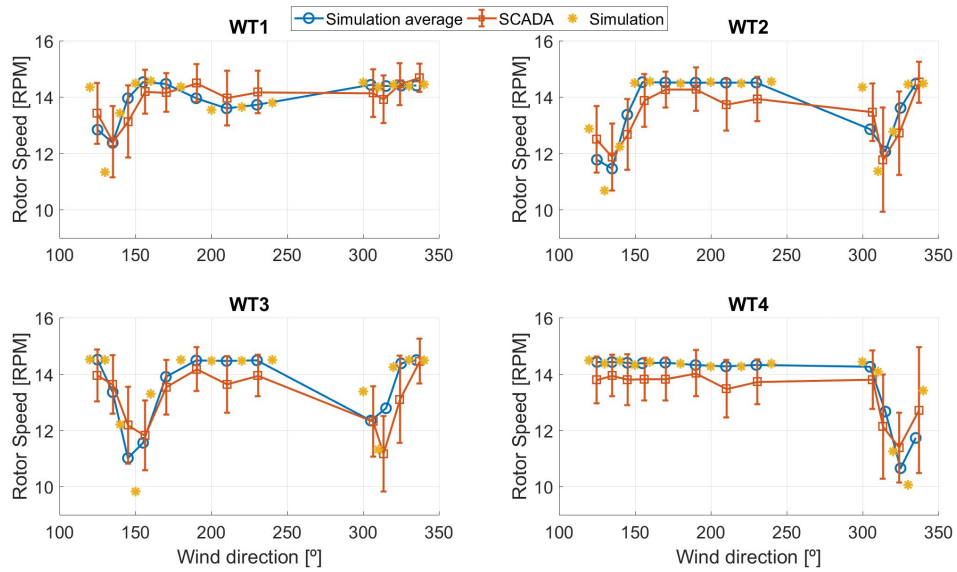


Figure 11: Mean rotor speed by direction, simulations vs SCADA data, for each wind turbine

## 6 Conclusion and Future Work

A Large Eddy Simulation framework with the Actuator Line Model to represent the wind turbine rotors has been used to simulate the operation of an onshore wind farm considering 14 different wind directions and subject to an ABL wind flow. The electric power and rotor speed simulation results were compared with SCADA data of the farm, finding good agreement between the mean values. Power and velocity deficits were well captured in the simulations.

Future research will focus on the use of this numerical framework to simulate this and other wind farms, considering various ABL profiles as inlet, to evaluate wind resource both at the design and operation stages of wind farms. The use of GPU computing platform as considered in [25] is now being expanded to the full flow solver, using a dual CUDA / OpenCL syntax on top of the coarse MPI parallelization. This approach allows achieving speed-ups of up to 30x with respect to the CPU only solver and will be next extended to the wind turbine module routines.

## References

- [1] Iea. Technology roadmap - Wind energy. *Technology Roadmap*, page 58, 2013.
- [2] GWEC. Global Wind Report 2015 | Gwec. *Wind energy technology*, page 75, 2016.
- [3] Yu Ting Wu and Fernando Porté-Agel. Modeling turbine wakes and power losses within a wind farm using LES: An application to the Horns Rev offshore wind farm. *Renewable Energy*, 75:945–955, 2015.
- [4] A. Guggeri, M. Draper, and G. Usera. Simulation of a 7.7 MW onshore wind farm with the Actuator Line Model. *Journal of Physics: Conference Series*, 854(1), 2017.
- [5] M. Sessarego, W.Z. Shen, M.P. van der Laan, K.S. Hansen, and W.J. Zhu. CFD simulations of flows in awind farm in complex terrain and comparisons to measurements. *Applied Sciences (Switzerland)*, 8(5):1–21, 2018.
- [6] Fernando Porté-Agel, Yu Ting Wu, Hao Lu, and Robert J. Conzemius. Large-eddy simulation of atmospheric boundary layer flow through wind turbines and wind farms. *Journal of Wind Engineering and Industrial Aerodynamics*, 99(4):154–168, 2011.
- [7] Matthew J Churchfield, Sang Lee, Patrick J Moriarty, Luis A Martinez, Stefano Leonardi, Ganesh Vijayakumar, and James G Brasseur. A large-eddy simulation of wind-plant aerodynamics. *AIAA paper*, 537:2012, 2012.
- [8] G Usera, A Vernet, and J A Ferré. A Parallel Block-Structured Finite Volume Method for Flows in Complex Geometry with Sliding Interfaces. *Flow, Turbulence and Combustion*, 81(3):471, 2008.
- [9] Mariana Mendina, Martin Draper, Ana Paula Kelm Soares, Gabriel Narancio, and Gabriel Usera. A general purpose parallel block structured open source incompressible flow solver. *Cluster Computing*, 17(2):231–241, 2014.
- [10] Joel H Ferziger and Milovan Peric. *Computational Methods for Fluid Dynamics*. Springer-Verlag Berlin Heidelberg, 3 edition, 2002.
- [11] Joseph Smagorinsky. General circulation experiments with the primitive equations: I. The basic experiment. *Monthly weather review*, 91(3):99–164, 1963.
- [12] Paul J Mason and D J Thomson. Stochastic backscatter in large-eddy simulations of boundary layers. *Journal of Fluid Mechanics*, 242:51–78, 1992.
- [13] Massimo Germano, Ugo Piomelli, Parviz Moin, and William H Cabot. A dynamic subgrid-scale eddy viscosity model. *Physics of Fluids A: Fluid Dynamics*, 3(7):1760–1765, 1991.
- [14] Yan Zang, Robert L Street, and Jeffrey R Koseff. A dynamic mixed subgrid-scale model and its application to turbulent recirculating flows. *Physics of Fluids A: Fluid Dynamics*, 5(12):3186–3196, 1993.
- [15] FERNANDO PORTÉ-AGEL, CHARLES MENEVEAU, and MARC B PARLANGE. A scale-dependent dynamic model for large-eddy simulation: application to a neutral atmospheric boundary layer. *Journal of Fluid Mechanics*, 415:261–284, 2000.
- [16] M Mendina, M Draper, A P Kelm Soares, G Narancio, and G Usera. A general purpose parallel block structured open source incompressible flow solver. *Cluster Computing*, 17(2):231–241, nov 2013.
- [17] M Draper. *Simulación del campo de vientos y de la interacción entre aerogeneradores*. PhD thesis, 2015.

- [18] M Draper and G Usera. Evaluation of the Actuator Line Model with coarse resolutions. *Journal of Physics: Conference Series*, 625(1):12021, 2015.
- [19] Yu-Ting Wu and Fernando Porté-Agel. Large-Eddy Simulation of Wind-Turbine Wakes: Evaluation of Turbine Parametrisations. *Boundary-Layer Meteorology*, 138(3):345–366, 2010.
- [20] M Draper, A Guggeri, and G Usera. Modelling one row of Horns Rev wind farm with the Actuator Line Model with coarse resolution. *Journal of Physics: Conference Series*, 753:82028, sep 2016.
- [21] M Draper, A Guggeri, and G Usera. Validation of the Actuator Line Model with coarse resolution in atmospheric sheared and turbulent inflow. *Journal of Physics: Conference Series*, 753:82007, sep 2016.
- [22] R J A M Stevens, L A Martinez-Tossas, and C Meneveau. Comparison of wind farm large eddy simulations using actuator disk and actuator line models with wind tunnel experiments. *Renewable Energy*, 116:470–478, 2018.
- [23] Wim Munters, Charles Meneveau, and Johan Meyers. Shifted periodic boundary conditions for simulations of wall-bounded turbulent flows. *Physics of Fluids*, 28(2), 2016.
- [24] Kurt S. Hansen, Rebecca J. Barthelmie, Leo E. Jensen, and Anders Sommer. The impact of turbulence intensity and atmospheric stability on power deficits due to wind turbine wakes at Horns Rev wind farm. *Wind Energy*.
- [25] Pablo Igounet, Pablo Alfaro, Gabriel Usera, and Pablo Ezzatti. Towards a finite volume model on a many-core platform. *International Journal of High Performance Systems Architecture* 12, 4(2):78–88, 2012.

**2.3. Paper 3: An Actuator Line Model Simulation of two semi-aligned wind turbine models, operating above-rated wind speed**

# An Actuator Line Model Simulation of two semi-aligned wind turbine models, operating above-rated wind speed

A. Guggeri\*, M. Draper\*, G. Usera\* and F. Campagnolo\*\*  
Corresponding author: aguggeri@fing.edu.uy

\* Facultad de Ingeniería, Universidad de la República,  
Julio Herrera y Reissig 565, Montevideo, Uruguay.

\*\* Wind Energy Institute, Technische Universität München,  
Boltzmannstraße 15, D-85748 Garching bei München, Germany.

**Abstract:** Wind energy is expanding rapidly worldwide, being horizontal axis wind turbines (HAWT) the technology of greater installed capacity. A characteristic of this technology is the need to limit the production of power when the wind speed is greater than the rated one. In this work we show results of a validated numerical method applied to the simulation of two model wind turbines operating at above rated wind speed, showing their ability to control the power output. Five different wind velocity profiles at the inlet of the simulations domain were considered. The results of one simulation are compared to data obtained from a well known wind tunnel campaign, finding good agreement between the temporal evolution of the involved variables.

*Keywords:* Actuator Line Model, LES, Wind Turbines, Power Control.

## 1 Introduction

In the last decades wind energy has had a very large expansion, being horizontal axis wind turbines (HAWT) the technology of greater installed capacity among renewable energies [1]. Due to the transient nature of the wind flow through a wind farm, the state-of-the-art methodology to simulate it consists of Large Eddy Simulations (LES), while two approaches exist in order to represent the presence of a wind turbine in a simulation: actuator models, in which the blades are represented as body forces, and direct representation of the blade's geometry through the computational mesh. Among the actuator models, the Actuator Line (AL) has been widely validated, taking into account different inflow conditions, showing to reproduce with reasonable accuracy the wind flow in the wake of a wind turbine with moderately computation cost. Some validation cases and applications of this methodology can be seen in [2] [3] [4] [5] [6] [7] [8] [9] [10]. To compute the aerodynamic forces along the blades, as well as integral quantities such as total power and thrust, an aero-elastic code, such as FAST [11] or FLEX5 [12] can be coupled to the LES-AL framework.

A characteristic of a HAWT is its capacity to control the active power production, when the wind speed up-stream of the rotor is greater than the rated one. To accomplish this, the wind turbines regulate the torque imposed by the electric generator and the angle of the blades (pitch), in order to control the angular speed of the rotor, and thus the power output [13] [14]. These turbine controllers may be implemented in the aero-elastic code, for example: in [15] the FAST code was coupled with a LES solver and an actuator disk to investigate wake structures and interaction effects between dynamically controlled turbines; in [16] the CFD code developed by NREL, SOWFA [4], was coupled with FAST, with individual controllers for each turbine and also with a super-controller, which enables control at wind plant level; in [17] the 3D general purpose flow solver, EllipSys3D [9] and the Actuator Line method are combined with FLEX5, which supports control algorithms for the generator and the pitch systems, although the focus of that work is not dynamically controlling the wind turbines.

Another approach to simulate the aerodynamics and controllers of the wind turbines is to directly implement them in the CFD code, rather than coupling with the aero-elastic model. Examples of this are given at [18], where the generator torque controller was implemented in the LES-AL framework VWis (Virtual Wind Simulator), and in [19] where a modeling framework is proposed and validated, combining LES, the actuator-disk model and a turbine-model-specific relationship between shaft torque and rotational speed, to simulate turbine wakes and associated power losses in wind farms.

In this work we present simulations of the wind flow and the operation of wind turbines (WT) operating at wind speeds above the rated one. To simulate the wind flow the validated CFD solver `caffa3d.MBRi` [20][21] was used, and the wind turbines were represented by the AL. A closed-loop active power controller, based on the one described in [22], was implemented directly in `caffa3d.MBRi` by adding a series of subroutines. This controller enables the operation of wind turbines in the whole range of wind speeds. For validation, the simulation results were compared to data obtained from a well known wind tunnel experimental campaign performed by the Wind Energy Institute of Technische Universität München (TUM). These tests were conducted within the boundary layer wind tunnel of the Politecnico di Milano [23], where a scaled wind farm, composed of two wind turbine models already used within other research projects [24, 25, 26], has been employed.

This work is a complement of the paper [27] also presented in this conference, in which simulations of the same model wind turbines were performed with the same CFD code, but considering another arrangement of the turbines and different operational conditions to those presented in the current paper. The rest of this paper is organized as follows: in the next Section the numerical model is described; Section 3 presents the wind tunnel campaign, used for validation of the simulations. In Section 4 the numerical setup of the simulations and the results are presented. Finally conclusions and future work are proposed in Section 5.

## 2 Numerical Model

### 2.1 CFD solver

`caffa3d.MBRi` [21] [20] is an open source, finite volume (FV) code, second order accurate in space and time, parallelized with MPI, in which the domain is divided in unstructured blocks of structured grids. The mathematical model comprises the mass balance equation (1) and momentum balance equation (2) for a viscous incompressible fluid, together with generic passive scalar transport equation (3) for scalar field  $\phi$  with diffusion coefficient  $\Gamma$ . Note that (2) has been written only for the first Cartesian direction  $\hat{e}_1$ . The balance equations are written for a region  $\Omega$ , limited by a closed surface  $S$ , with outward pointing normal  $\hat{n}_S$ .

$$\int_S (\vec{v} \cdot \hat{n}_S) dS = 0 \quad (1)$$

$$\int_{\Omega} \rho \frac{\partial u}{\partial t} d\Omega + \int_S \rho u (\vec{v} \cdot \hat{n}_S) dS = \int_{\Omega} \rho \beta (T - T_{ref}) \vec{g} \cdot \hat{e}_1 d\Omega + \int_S -p \hat{n}_S \cdot \hat{e}_1 dS + \int_S (2\mu D \cdot \hat{n}_S) \cdot \hat{e}_1 dS \quad (2)$$

$$\int_{\Omega} \rho \frac{\partial \phi}{\partial t} d\Omega + \int_S \rho \phi (\vec{v} \cdot \hat{n}_S) dS = \int_S \Gamma (\nabla \phi \cdot \hat{n}_S) dS \quad (3)$$

where  $\vec{v} = (u, v, w)$  is the fluid velocity,  $\rho$  is the density,  $\beta$  is the thermal expansion factor,  $T$  is the fluid temperature and  $T_{ref}$  a reference temperature,  $\vec{g}$  is the gravity,  $p$  is the pressure,  $\mu$  is the dynamic viscosity of the fluid and  $D$  is the strain tensor. The use of equations in their global balance form, together with the finite volume method, as opposed to the differential form, favors enforcing conservation properties for fundamental magnitudes as mass and momentum into the solving procedure [28].

To deal with the linearization and subsequent coupling of linear systems for each equation in the mathematical model, an outer-inner iteration scheme for each time step is employed, as shown in Figure 1. Linear systems for each equation in the mathematical model are sequentially assembled and undergo inner iterations with SIP or AMG-SIP linear solvers. The outer loop is repeated within each time step until the desired level of convergence is achieved before continuing to the next time step.

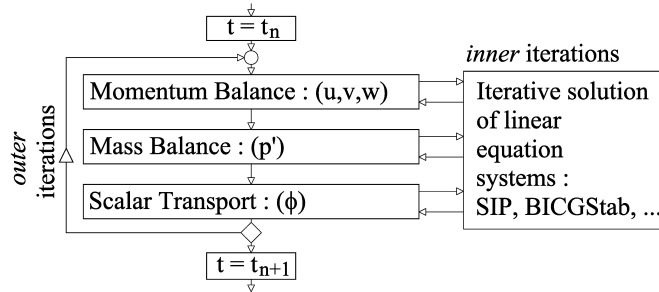


Figure 1: Iteration scheme for one time step (adapted from [28]).

Representation of complex geometries can be handled through a combination of body fitted grids and the immersed boundary method over both Cartesian and body fitted grid blocks. Geometrical properties and flow properties, which are expressed in primitive variables, are always expressed in a Cartesian coordinate system, using a collocated arrangement. Regarding the turbulence model, different subgrid scale models in the context of Large Eddy Simulation (LES) are implemented: the standard Smagorinsky model [29] with damping function for smooth [28] and rough surfaces [30], the dynamic Smagorinsky model [31] with different averaging schemes, the dynamic mixed Smagorinsky model [32] and the scale-dependent dynamic Smagorinsky model [33] with different averaging schemes. Further details of the solver together with validations can be found in [21, 20].

## 2.2 Actuator Line Model

The ALM has been implemented in the code [34] to represent wind turbines rotors in the simulations. Despite it is recommended to use a spatial resolution of at least  $R/30$  and to set the time step size in order to limit the movement of the rotor tip to a grid cell length in each time step [14], the ALM has been evaluated with coarser resolutions [35] [34] [36] [37] [38] [39], still obtaining acceptable results.

Each blade is represented as a line that moves with the rotational speed of the rotor and it is discretized in radial sections where the aerodynamic forces are computed (Figure 2, left). The geometrical properties of the blades (chord length and twist angle ( $\beta$ ) as well as aerodynamic properties (lift and drag coefficients) are necessary to compute the force in each radial section. The former are obtained directly from the model wind turbine, while the aerodynamic coefficients are computed from tabulated data of the corresponding airfoil. At each radial section the aerodynamic force is computed as

$$\vec{f} = -\frac{1}{2}\rho V_{rel}^2 c(C_L \vec{e}_L + C_D \vec{e}_D) dr \quad (4)$$

where  $\rho$  is the air density,  $V_{rel}$  is the relative velocity,  $c$  is the chord length,  $C_L$  is the lift coefficient,  $C_D$  is the drag coefficient,  $\vec{e}_L$  is a unit vector in the direction of the lift force,  $\vec{e}_D$  is a unit vector in the direction of the drag force and  $dr$  is the length of the radial section (see Figure 2, right). Prandtl's tip loss correction factor is applied, as it has shown to improve the results [35].

After computing the aerodynamic forces, it is required to project them onto the computational domain as a body force field. To accomplish this, a smearing Gaussian function is used, taking into account the distance between each grid cell and radial section, and three smearing parameters, one for each direction ( $n$  normal,  $r$  radial and  $t$  tangential).

$$f(d_n, d_r, d_t) = \frac{1}{\epsilon_n \epsilon_r \epsilon_t \pi^{1.5}} e^{-\left(\frac{d_n}{\epsilon_n}\right)^2} e^{-\left(\frac{d_r}{\epsilon_r}\right)^2} e^{-\left(\frac{d_t}{\epsilon_t}\right)^2} \quad (5)$$

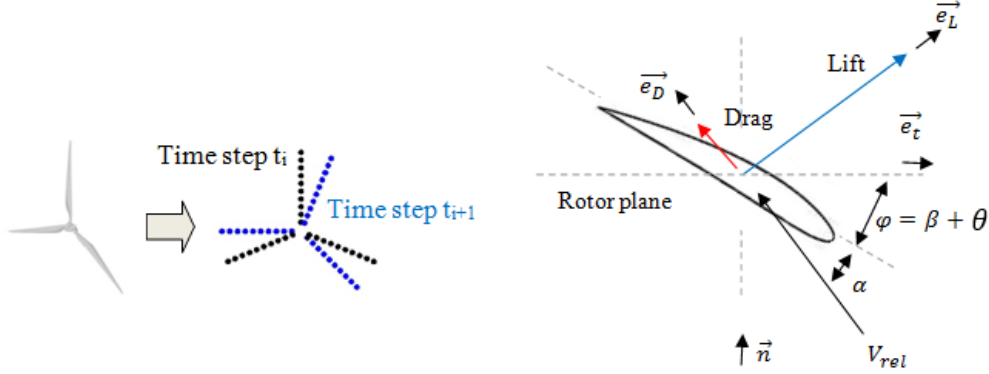


Figure 2: ALM rotor representation (left) and a cross-sectional airfoil radial section (right).

### 2.3 Power Control System

At each time step of the simulation, the resulting aerodynamic torque applied to the rotor shaft ( $M_{aero}$ ) is computed by integration of the tangential forces along the blades, and the rotational speed is obtained from the rotor second cardinal equation (6), where  $M_{gen}$  is the generator torque,  $\omega$  is the angular speed of the rotor at the current time step,  $I$  is the sum of the rotor, shaft and generator inertia considered at the low-speed side.  $\Delta t$  corresponds to the temporal step and  $\omega_{t-1}$  accounts for the rotational speed of the previous time step. It is worth mentioning that in each external iteration (see Figure 1) the aerodynamic torque is computed and a different value may be obtained, so a different angular speed may also be obtained. On the other side, to compute the generator torque and update the position of the blades, the rotational speed is needed, but those quantities should be kept constant along the external iterations, as they belong to the same time step. To solve this issue, only the angular speed of the first external iteration is considered to compute the mentioned variables, then keeping their values constant for the rest of the external iterations, regardless of the value the rotor speed might take in later iterations.

$$I \frac{d\omega}{dt} = M_{aero} - M_{gen} \Rightarrow \omega = \frac{(M_{aero} - M_{gen})}{I} \Delta t + \omega_{t-1} \quad (6)$$

Finally, the aerodynamic and electric power are calculated as the rotational speed multiplied by the shaft aerodynamic torque and the generator torque, respectively (equation 7).

$$\begin{aligned} P_{aero} &= M_{aero} \cdot \omega \\ P_{electric} &= M_{gen} \cdot \omega \end{aligned} \quad (7)$$

A basic characteristic of HAWTs is their ability to control the power output [22], when they are subject to the natural spacial and temporal variations of the wind speed flow, and as consequence to the variation of the forces acting on the rotor. The conventional approach to accomplish this is the design of two control systems which work independently, at the below-rated and above-rated wind-speed range. Respectively, these systems are the generator-torque controller, whose objective is to maximize power capture below the rated operation point, and the rotor-collective blade-pitch controller, with the goal of regulating the generator speed, and thus the rotor angular speed, at the rated operation point [13].

At the below-rated wind speed range, usually called Region 2, the generator torque is computed as a tabulated function, according to equation 8, where  $K$  is a constant that optimizes the power extraction from the wind and which depends on the aerodynamics and geometrical characteristics of the blades. The pitch-angle of the blades is fixed at its minimum value, in order to optimize the power extraction from the wind.

$$M_{gen} = K\omega^2 \quad (8)$$

At the above-rated wind-speed range, Region 3,  $M_{gen}$  is kept constant at its rated value. The rotor-collective blade-pitch-angle values are computed using a gain-scheduled proportional-integral (PI) control on the speed error ( $\Delta\omega$ ) between the current WT speed and the rated speed ( $\omega_{rated}$ ). In equation 9,  $\theta$  is the pitch angle (see Figure 2),  $K_I$  and  $K_P$  account for the proportional and integral gains respectively. The integral term accounts for the accumulated error over time, and in the simulations is computed by simply adding  $\Delta\omega$  to its previous value, in each time step. The pitch-angle values and its rate of change are limited by saturation values. This PI controller ensures that  $\omega$  fluctuates around its reference value, and so the active power output fluctuates around the active power rated value,  $P_{ref}$ . Figure 3 shows a flowchart of the control system that was implemented in the code.

$$\theta = K_P\Delta\omega + K_I \int_0^t \Delta\omega dt \quad (9)$$

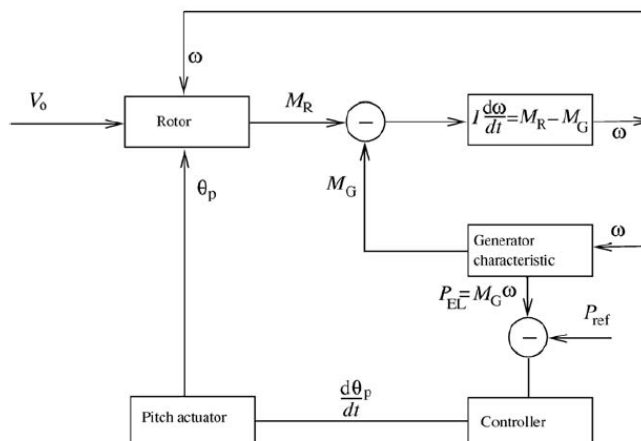


Figure 3: Active power control block diagram (extracted from [13])

### 3 Experimental Campaign

The experimental setup consisted of 2 wind turbine models, in the following named G1s, whose rotor diameter (D) is 1.1m and their hub height (HH) is 0.825m. They were separated  $4D$  in the streamwise direction and with a lateral shift of half a diameter. The undisturbed wind speed was measured by means of a Pitot tube, placed at hub height in front of the upstream model.

Each G1 is equipped with a three-blades rotor whose rated rotating speed is 850 . Each carbon-made blade, mounted on the hub with two bearings, houses, within its hollow root, a small brushed motor equipped with a gear-head and a built-in relative encoder. This system enables, together with a dedicated electronic control board housed in the hub spinner, the individual pitch angle variation of the blade. The combined inertia of the rotor, shaft and generator considered at the low-speed side is  $I = 1.39 \times 10^{-2} kg.m^2$

The model is controlled by a *M1 Bachmann* hard-real-time module. Similarly to what is done on real wind turbines, the *M1* implements collective or individual pitch-torque control laws, similar to the ones described in [40] and references therein. For the generator torque controller (see equation 8),  $K = 3.66 \times 10^{-6} \frac{N.m.s^2}{rad^2}$ . A more detailed description of the G1 and the wind tunnel can be found in [27]

## 4 Simulations setup and results

In this Section the numerical setup of the simulations and their results are presented. First a comparison of one simulation with the experimental data is done, and secondly we analyze simulations performed with 5 different ABL profiles as inlets.

### 4.1 Numerical setup

The size of the computational domain is 27.50m in the streamwise direction, 5.50m in the spanwise direction and 4.50m in the vertical direction. It is uniformly divided in the streamwise and spanwise direction with 384 and 96 grid cells respectively, while a stretched grid is used in the vertical direction with 80 grid cells, covering one vertical rotor diameter with 30 grid cells. In [27] two additional spatial resolutions have been tested for a stand-alone model wind turbine with the same numerical setup, obtaining an acceptable agreement with experimental data using the spatial resolution considered in the current paper. The Crank-Nicolson scheme is used to advance in time with a step of 0.005 seconds. 5000 time steps are simulated, which means 25 seconds of the G1s operation and accounts for approximately 300 turns of their rotor. The scale dependent dynamic Smagorinsky model with local averaging scheme is used to compute the sub-grid scale stress, as in previous studies [35, 37] better results were obtained with this sub-grid scale model. The model wind turbine is placed  $2D$  from the inlet. For further details on the numerical setup, please see [27].

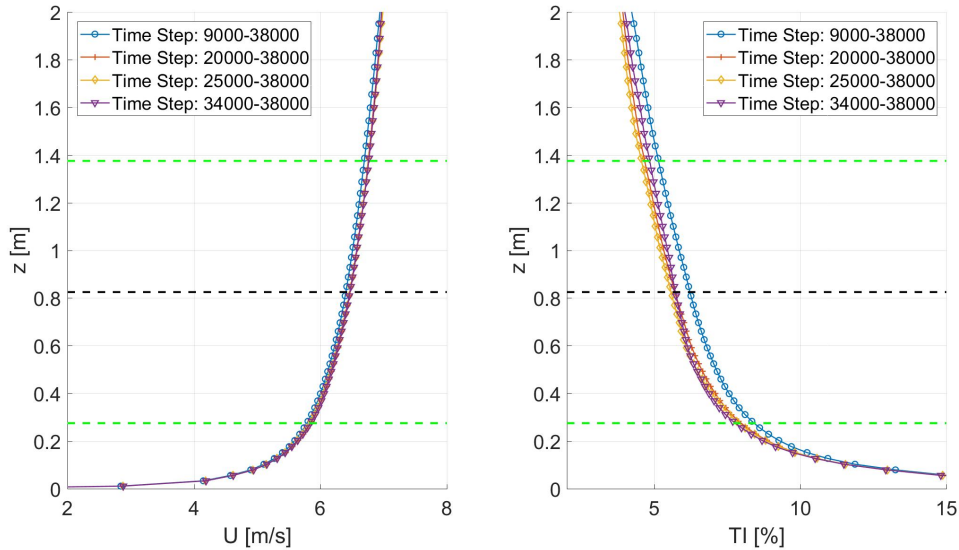


Figure 4: Span-wise averaged vertical profiles, at different time steps. Left: stream-wise velocity component ( $U$ ), right: stream-wise turbulence intensity ( $TI$ ). The black and green dotted lines represents the WT hub height and blades tip, respectively

The 2 wind turbine arrangement described in Section 3 was simulated subject to different ABL inflow conditions. These were obtained from precursor simulations, taking into account the same numerical setup described previously, but without wind turbines and applying a periodic boundary condition in the west and east boundaries and a constant pressure gradient as forcing term. After statistical convergence is reached, the velocity flow is considered at the inlet of the simulation with HAWTs. Figure 4 shows span-wise averages of the down-stream velocity component ( $U$ ) and of the turbulent intensity ( $TI$ ) vertical profiles, between different time steps of one precursor simulation. The turbulent intensity is calculated considering the stream-wise velocity component, according to equation 10, where  $\sigma(U)$  is the standard deviation of  $U$ .

$$TI = \sigma(U)/\bar{U} \quad (10)$$

The ABL profile shown in Figure 4 has a mean streamwise velocity component of 6.4m/s at hub height, a streamwise turbulence intensity of approx. 5.9% and is characterized by a power law with shear exponent of 0.1. Notice that after 20.000 time steps, the variation of U and TI vertical profiles is negligible, and thus convergence is achieved. At the experimental campaign U was 6.1m/s and TI = 3.7%, obtained from the Pitot tube measurements, which accounts for 5% difference in velocity at hub-height with respect to the simulation.

## 4.2 Results

In this Section the results of the simulations are presented: first, the data obtained from one simulation is compared with data from the experimental campaign described in 3, and secondly the influence of considering different wind flows at the inlet of the simulations is depicted.

To avoid the transient effect on the flow produced by the sudden inclusion of the turbines in the domain, the first 1000 time steps of the simulation, equivalent to 5 seconds, are discarded in the results shown and to calculate temporary averages of the G1 signals. The considered signals are the downstream velocity component (U), the rotor angular speed, the blade-pitch-angle and the active power output, both aerodynamic and electric. A comparison of the temporal evolution of the signals between the experimental and numerical data of the first WT can be seen in Figure 5.

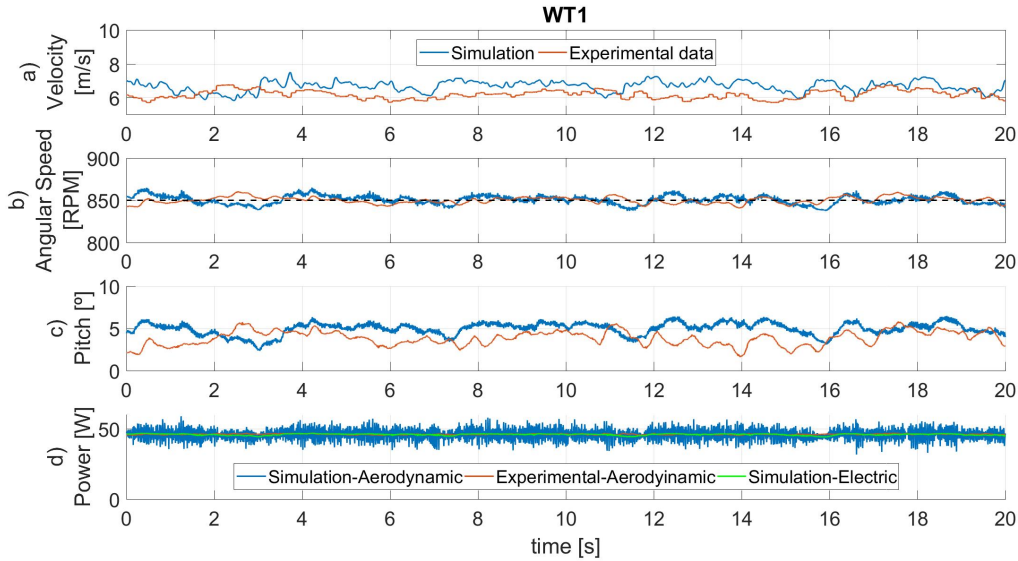


Figure 5: Temporal evolution of Wind Speed (top) Rotational Speed (middle-top), Pitch angle (middle-bottom) and Power production (bottom) of the first WT

Good agreement is found in the mean value of all the signals, with a slight overestimation of the pitch. The difference in wind velocity, being higher in the simulation, may explain this difference, as the aerodynamic torque is higher and thus a greater pitch angle is required to regulate the rotor speed. Also, larger fluctuations can be noticed when comparing the simulation aerodynamic power with the measured one. Although the higher TI at the inlet of the simulations may contribute to these difference, the reasons are not clear yet. On the other side, if the electric power output is considered, represented as the dotted green line and calculated as equation 7, the fluctuations are significantly reduced. It can be noticed that the angular speed signal fluctuates around the rated value, 850RPM, represented by the dotted black line.

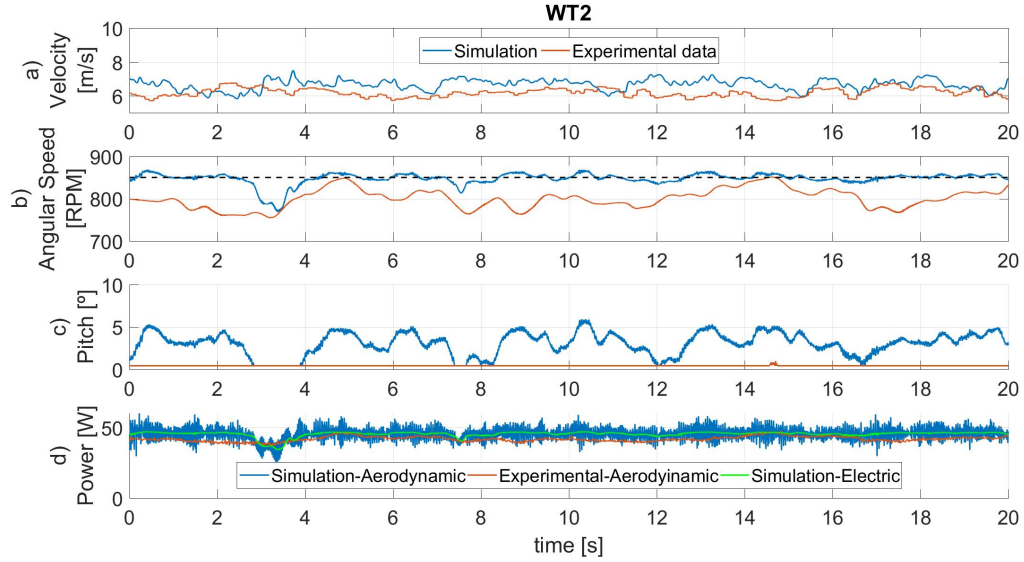


Figure 6: Temporal evolution of Wind Speed (top) Rotational Speed (middle-top), Pitch angle (middle-bottom) and Power production (bottom) of the second WT

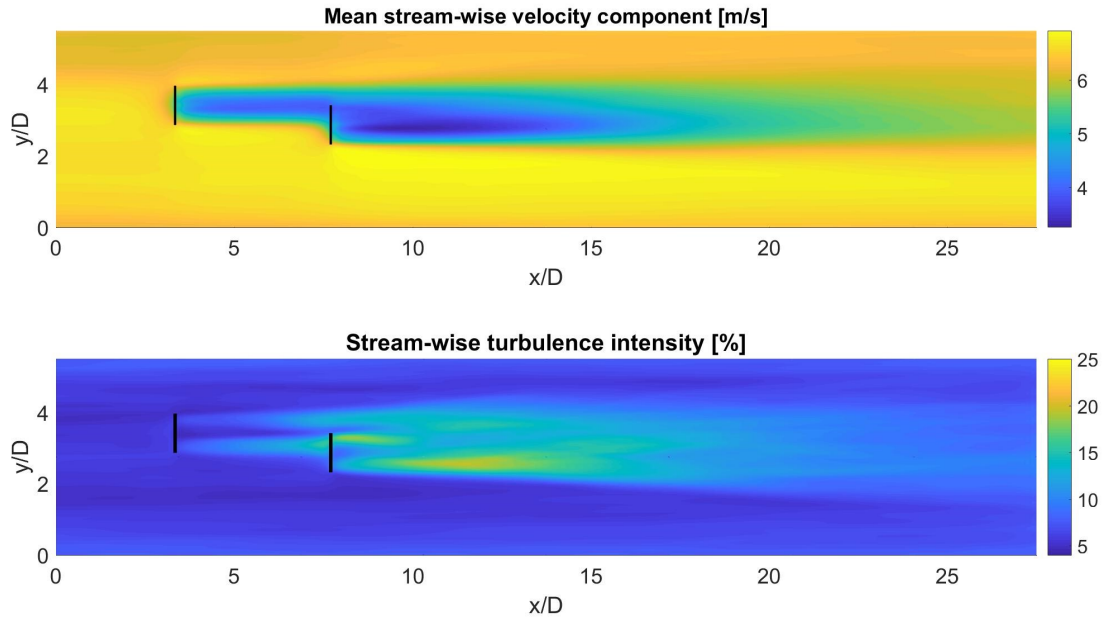


Figure 7: Mean stream-wise velocity component (top) and mean stream-wise turbulence intensity (bottom) on a horizontal plane at hub height. The wind turbines are represented by the black lines

On the other side, the second WT presents higher differences in all three signals, as it can be seen in Figure 6. Although no measurements of the velocity upstream of the second WT were taken in the experimental campaign, we suppose that the velocity deficit induced by the first WT may have been considerably lower

than the one obtained in the simulation. Again, the main reason for this could be the difference in velocity at the inlet between the simulation and the experimental data, which caused that in the experimental campaign the second G1 rarely reached its rated rotational speed, while in the simulation it does, and explains why the pitch-angle was kept constant at its minimum value and why the measured power is overestimated by 8%. Notice that the velocity signal in Figure 6 is the same as in Figure 5, and it corresponds to the Pitot tube measurement for the experimental, and to the span-wise average of the velocity at cells located in the inlet at hub height and upstream of the first WT, for the simulation data.

Figure 7 shows the mean stream-wise velocity component and turbulence intensity (TI) on a horizontal plane at hub height. That figure shows the wake deficit downstream the rotor, characterized by a large velocity deficit in the wake center and extending beyond  $10D$  downstream, and an increase in TI, particularly at the blade tips.

To test the power controller at wind velocities higher than the rated one, the 2 wind turbines arrangement was simulated subject to four other ABL inflow conditions. Figure 8 depicts the mean stream-wise velocity component ( $U$ ) and TI, at the inlet and averaged along the span-wise direction. Inlet 2 corresponds to the simulation presented previously in this section. Table 1 depicts  $U$  and TI at hub height (HH) for each simulation

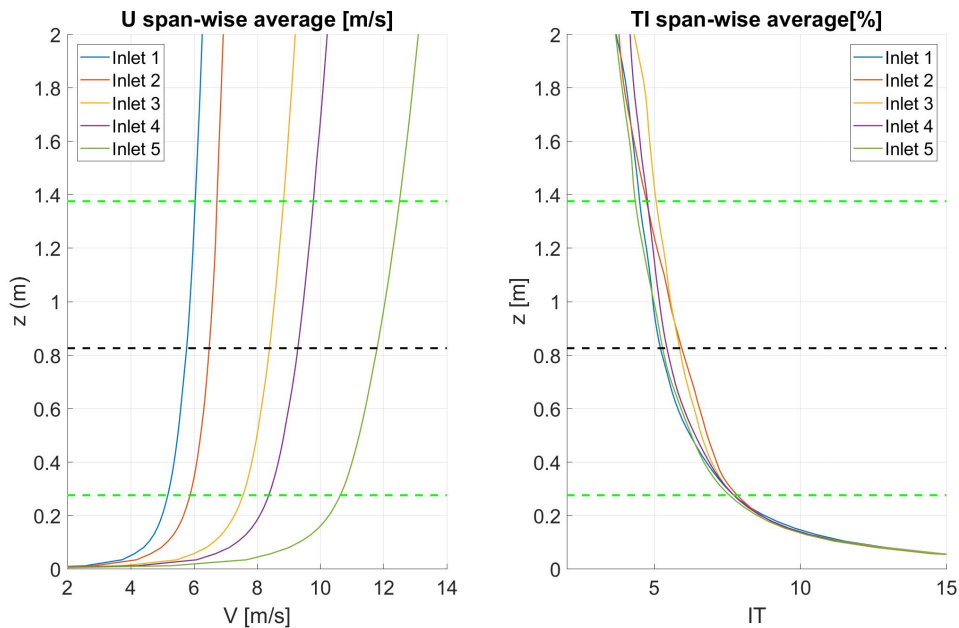


Figure 8: Span-wise averaged vertical profiles of the five simulation's inlets. Left: stream-wise velocity component ( $U$ ), right: stream-wise turbulence intensity (TI). The black and green dotted lines represents the G1s hub height and blades tip, respectively

The temporal mean values of power, power coefficient ( $CP$ ) and pitch angles were computed and plotted against the mean stream-wise velocity component at hub height, for both wind turbines. This is shown in Figure 9, where the experimental data are included considering the wind velocity measured by the Pitot.

The mean power coefficient is calculated according to equation 11. In this equation,  $U$  represents the average of the velocity in cells at the inlet, at hub height and up-stream of the first WT. The reason to consider only these cells and not the whole span-wise direction, is that as it can be noticed on Figure 7, the velocity at the inlet is not uniform along span-wise variation, with a difference of 10% between the maximum and minimum value at hub height. Particularly, in the cells of the domain located up-stream of the first WT there is a zone of higher velocities. The same was noticed at the experimental campaign, where a difference in velocity of 6% along the span-wise section was reported in [41]. In equation 11,  $P$  accounts for the electric

Table 1: U and TI of inlets at hub height.

Profile	$U_{HH}$ [m/s]	$TI_{HH}$ [%]
Inlet 1	5.8	5.2
Inlet 2	6.5	5.9
Inlet 3	8.4	5.8
Inlet 4	9.3	5.4
Inlet 5	11.8	5.3

power,  $\rho$  the air density,  $1.2\text{kg/m}^3$  and  $A$  the area swept by the rotor, equivalent to  $D^2\pi/4$ . Notice that the same wind velocity is considered to calculate the  $CP$  of both wind turbines, although the second G1 is located in the wake of the first one, and thus the velocity is significantly lower. This difference in velocity leads to a  $CP$  lower to what is expected for the second turbine, which is operating below rated wind speed.

$$CP = \left\langle \frac{P}{0.5U^3\rho A} \right\rangle = \left\langle \frac{8P}{U^3\rho D^2\pi} \right\rangle \quad (11)$$

Good agreement is found in the the experimental and simulated  $CP$  of the first G1. For the second wind turbine, the interpolated value of the mean power coefficient is 0.284, which has a difference of 7% compared to the 0.304 of the experimental data. Again, the main reason for this difference may be caused by the sensibility of the  $CP$  to the reference velocity ( $U$ ), which has significant span-wise variation both in the simulation and in the experiments.

In Figure 9 it can be observed that for velocities higher than the rated one, both G1s operate at rated power and the power coefficient decreases while the pitch angle increases, as it is expected for the operation of pitch-controlled wind turbines, according to [13]

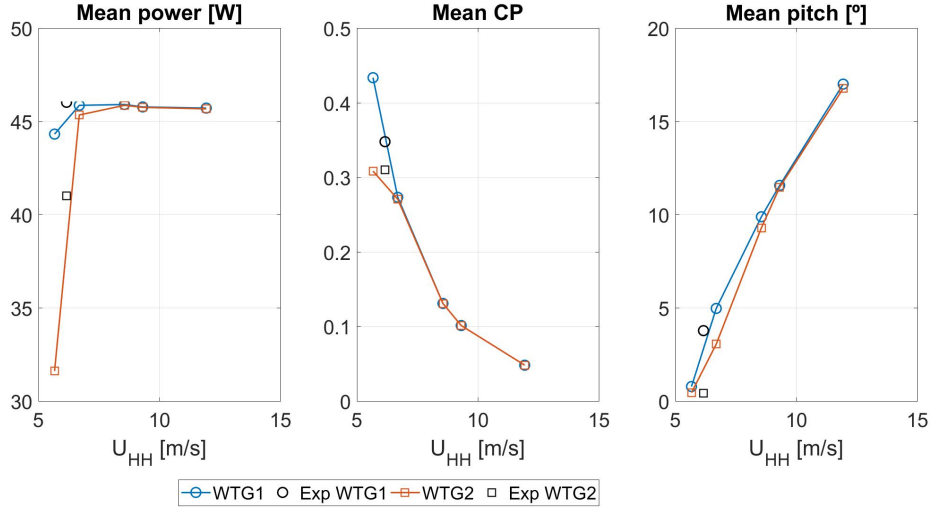


Figure 9: Mean power, CP and pitch vs mean stream-wise velocity at hub height

The temporal evolution of the variables of the first and second WT are depicted in Figures 10 and 11. Inlet 1 has a mean stream-wise velocity component at hub height of 5.8m/s, which is slightly lower than Inlet 2, and causes that the first WT occasionally does not reach its rated speed, and in those cases the pitch

is kept constant at its minimum value. For the second WT it is clear that it does not reach rated speed, and its operation resembles to what is observed in the experimental campaign (see Figure 6). For the rest of the simulations, with higher wind velocity at the inlet, both the rotor speed and the power output oscillates around the rated value, for both wind turbines, which proves that the power controller works correctly.

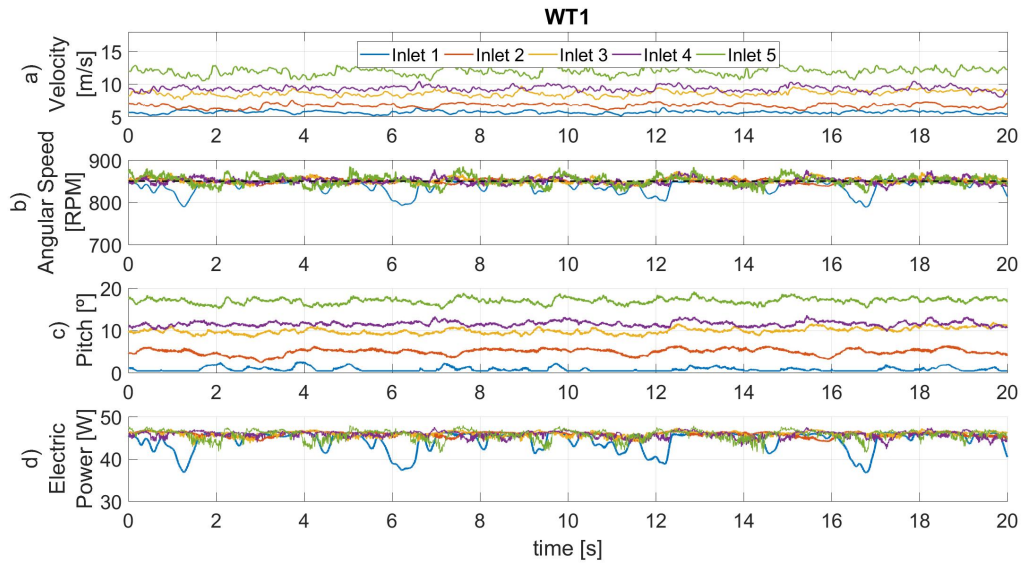


Figure 10: Temporal evolution of simulation signals of the first WT

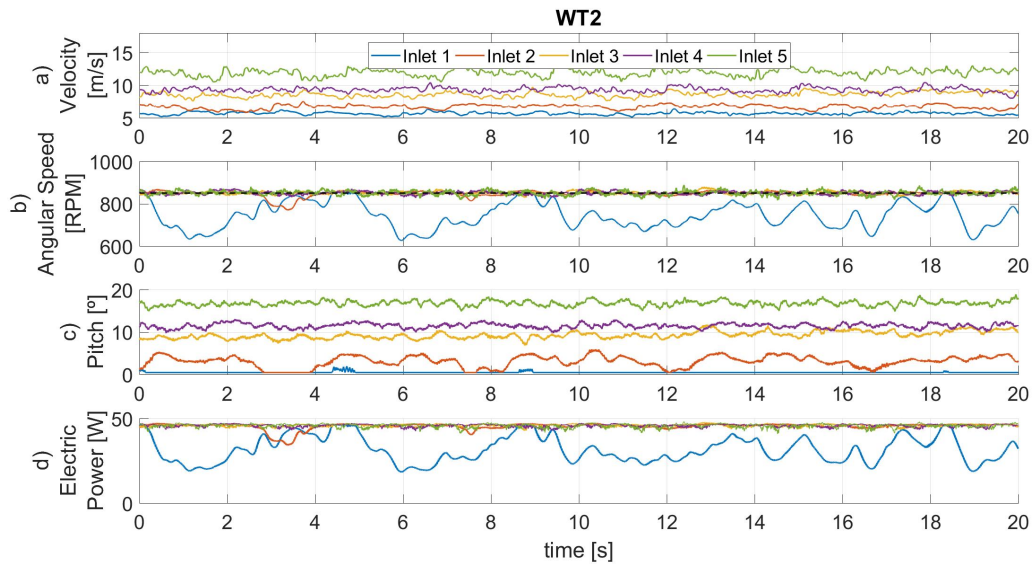


Figure 11: Temporal evolution of simulation signals of the second WT

## 5 Conclusion and Future Work

A Large Eddy Simulation framework with the Actuator Line Model to represent the wind turbine rotors has been used to simulate the operation of a two semi-aligned wind turbine arrangement, subject to five different ABL wind profiles with hub height velocities close or higher than the rated one. The results of the simulations were compared to an experimental campaign developed at Politecnico di Milano wind tunnel.

A closed-loop collective-pitch and a torque controller was implemented in the CFD code, as a series of subroutines. This allowed to simulate the whole range of operation of the wind turbines. In general, an acceptable agreement is obtained between the mean values of the experimental data and the numerical results, although significant differences in the amplitude of the signal of aerodynamic power were found when comparing the experimental and simulation data. The reasons for this are not clear yet, and we plan to keep investigating them.

Future research will focus on the use of this numerical framework to study wind farm control strategies, both for maximizing power production and for active power control. The use of GPU computing platform as considered in [42] is now being expanded to the full flow solver, using a dual CUDA / OpenCL syntax on top of the coarse MPI parallelization. This approach allows achieving speedups of up to 30x with respect to the CPU only solver and will be next extended to the wind turbine module routines.

## References

- [1] GWEC. Global Wind Report 2015 | Gwec. *Wind energy technology*, page 75, 2016.
- [2] J N Sorensen and W Z Shen. Numerical Modeling of Wind Turbine Wakes. *Journal of Fluids Engineering*, 124(2):393, 2002.
- [3] F Porté-Agel, H Lu, and YT Wu. A large-eddy simulation framework for wind energy applications. *Fifth International Symposium on . . .*, 2010.
- [4] M Churchfield, S Lee, P Moriarty, L Martinez, S Leonardi, Ganesh Vijayakumar, and James Brasseur. A Large-Eddy Simulations of Wind-Plant Aerodynamics. *50th AIAA Aerospace Sciences Meeting including the New Horizons Forum and Aerospace Exposition*, 2012.
- [5] P K Jha, M J Churchfield, P J Moriarty, and Sven Schmitz. Accuracy of state-of-the-art actuator-line modeling for wind turbine wakes. *AIAA Paper*, (2013-0608), 2013.
- [6] N Troldborg, J Nørkær, and R Flemming. *Actuator Line Modeling of Wind Turbine Wakes by N Troldborg Dissertation submitted to the Technical University of Denmark in partial fulfillment of*. 2009.
- [7] L A Mart\`inez-Tossas, M J Churchfield, and S Leonardi. Large eddy simulations of the flow past wind turbines: actuator line and disk modeling. *Wind Energy*, 18(6):1047–1060, 2014.
- [8] N Troldborg, F Zahle, P E Réthoré, and N N Sørensen. Comparison of wind turbine wake properties in non-sheared inflow predicted by different computational fluid dynamics rotor models. *Wind Energy*, 18(7):1239–1250, 2015.
- [9] S Ivanell, R Mikkelsen, J N Sørensen, and D Henningson. Validation of methods using EllipSys3D. pages 183–221, 2008.
- [10] R J A M Stevens, L A Mart\`inez-Tossas, and C Meneveau. Comparison of wind farm large eddy simulations using actuator disk and actuator line models with wind tunnel experiments. *Renewable Energy*, 116:470–478, 2018.
- [11] J. M. Jonkman and M. L. Jr. Buhl. FAST User’s Guide - Updated August 2005. (October), 2005.
- [12] Stig Øye. Dynamisk, aeroelastisk beregning af vindmøllevinger. Technical report, DTU, 1983.
- [13] K S Hansen, R J Barthelmie, L E Jensen, and A Sommer. The impact of turbulence intensity and atmospheric stability on power deficits due to wind turbine wakes at Horns Rev wind farm. *Wind Energy*.
- [14] T Burton, N Jenkins, D Sharpe, and E Bossanyi. *Wind Energy Handbook*. 2011.
- [15] R Storey and SE Norris. Large Eddy Simulation of Dynamically Controlled Wind Turbines. *Ewea Offshore 2011*, (January):1–10, 2011.
- [16] P Fleming, S Lee, M Churchfield, A Scholbrock, J Michalakes, K Johnson, and P Moriarty. The SOWFA Super-Controller : A High-Fidelity Tool for Evaluating Wind Plant Control Approaches. *European Wind Energy Association 2013*, (January), 2013.

- [17] R Mikkelsen, Jens N. Sørensen, Stig Øye, and N Troldborg. Analysis of power enhancement for a row of wind turbines using the actuator line technique. *Journal of Physics: Conference Series*, 75(1), 2007.
- [18] Xiaolei Yang, Jennifer Annoni, Pete Seiler, and Fotis Sotiropoulos. Modeling the effect of control on the wake of a utility-scale turbine via large-eddy simulation. In *Journal of Physics: Conference Series*, volume 524, page 12180. IOP Publishing, 2014.
- [19] Y Wu and F Porté-Agel. Modeling turbine wakes and power losses within a wind farm using LES: An application to the Horns Rev offshore wind farm. *Renewable Energy*, 75:945–955, 2015.
- [20] M Mendina, M Draper, A P Kelm Soares, G Narancio, and G Usera. A general purpose parallel block structured open source incompressible flow solver. *Cluster Computing*, 17(2):231–241, 2014.
- [21] G Usera, A Vernet, and J A Ferré. A Parallel Block-Structured Finite Volume Method for Flows in Complex Geometry with Sliding Interfaces. *Flow, Turbulence and Combustion*, 81(3):471, 2008.
- [22] J Jonkman, S Butterfield, W Musial, and G Scott. Definition of a 5-MW Reference Wind Turbine for Offshore System Development. (February), 2009.
- [23] C L Bottasso, F Campagnolo, and V Petrović. Wind tunnel testing of scaled wind turbine models: Beyond aerodynamics. *Journal of Wind Engineering and Industrial Aerodynamics*, 127(Supplement C):11–28, 2014.
- [24] F Campagnolo, V Petrović, J Schreiber, E M Nanos, A Croce, and C L Bottasso. Wind tunnel testing of a closed-loop wake deflection controller for wind farm power maximization. *Journal of Physics: Conference Series*, 753:32006, sep 2016.
- [25] F Campagnolo, V Petrović, C L Bottasso, and A Croce. Wind tunnel testing of wake control strategies. In *2016 American Control Conference (ACC)*, pages 513–518, 2016.
- [26] F Campagnolo, V Petrović, E Nanos, C Tan, C L Bottasso, I Paek, and H Kim K Kim. Wind tunnel testing of power maximization control strategies applied to a multi-turbine floating wind power platform. In *Proceedings of the International Offshore and Polar Engineering Conference*, 2016.
- [27] M Draper, A Guggeri, M Mendina, G Usera, and F Campagnolo. A Large Eddy Simulation model for the study of wind turbine interactions and its application. In *10th International Conference on Computational Fluid Dynamics , Barcelona, Accepted for presentation*, 2018.
- [28] J H Ferziger and M Peric. *Computational Methods for Fluid Dynamics*. Springer-Verlag Berlin Heidelberg, 3 edition, 2002.
- [29] J Smagorinsky. General circulation experiments with the primitive equations: I. The basic experiment. *Monthly weather review*, 91(3):99–164, 1963.
- [30] P J Mason and D J Thomson. Stochastic backscatter in large-eddy simulations of boundary layers. *Journal of Fluid Mechanics*, 242:51–78, 1992.
- [31] M Germano, U Piomelli, P Moin, and W H Cabot. A dynamic subgrid-scale eddy viscosity model. *Physics of Fluids A: Fluid Dynamics*, 3(7):1760–1765, 1991.
- [32] Y Zang, R L Street, and J R Koseff. A dynamic mixed subgrid-scale model and its application to turbulent recirculating flows. *Physics of Fluids A: Fluid Dynamics*, 5(12):3186–3196, 1993.
- [33] F Porté-Agel, C Meneveau, and M B Parlange. A scale-dependent dynamic model for large-eddy simulation: application to a neutral atmospheric boundary layer. *Journal of Fluid Mechanics*, 415:261–284, 2000.
- [34] M Draper. *Simulación del campo de vientos y de la interacción entre aerogeneradores*. PhD thesis, 2015.
- [35] M Draper and G Usera. Evaluation of the Actuator Line Model with coarse resolutions. *Journal of Physics: Conference Series*, 625(1):12021, 2015.
- [36] M Draper, A Guggeri, and G Usera. Validation of the Actuator Line Model with coarse resolution in atmospheric sheared and turbulent inflow. *Journal of Physics: Conference Series*, 753(8), 2016.
- [37] M Draper, A Guggeri, and G Usera. Modelling one row of Horns Rev wind farm with the Actuator Line Model with coarse resolution. *Journal of Physics: Conference Series*, 753(8), 2016.
- [38] M Draper, A Guggeri, and G Usera. Modelling one row of Horns Rev wind farm with the Actuator Line Model with coarse resolution. *Journal of Physics: Conference Series*, 753:82028, sep 2016.
- [39] A Guggeri, M Draper, and G Usera. Simulation of a 7.7 MW onshore wind farm with the Actuator Line Model. *Journal of Physics: Conference Series*, 854(1), 2017.
- [40] E A Bossanyi. The Design of closed loop controllers for wind turbines. *Wind Energy*, 3(3):149–163, 2000.
- [41] J Wang, S Foley, E M Nanos, T Y, F Campagnolo, C L Bottasso, A Zanotti, and A Croce. Numerical

- and Experimental Study of Wake Redirection Techniques in a Boundary Layer Wind Tunnel. *Journal of Physics: Conference Series*, 854:12048, may 2017.
- [42] P Igounet, P Alfaro, G Usera, and P Ezzatti. Towards a finite volume model on a many-core platform. *International Journal of High Performance Systems Architecture* 12, 4(2):78–88, 2012.

**2.4. Paper 4: Actuator Line Model simulations to study active power control at wind turbine level**

# Actuator Line Model simulations to study active power control at wind turbine level

**Andrés Guggeri, Martín Draper, Bruno López and Gabriel Usera**

Universidad de la República, Facultad de Ingeniería, Instituto de Mecánica de los Fluidos e Ingeniería Ambiental, Julio Herrera y Resissig 565, Montevideo, Uruguay

E-mail: [aguggeri@fing.edu.uy](mailto:aguggeri@fing.edu.uy)

**Abstract.** Wind energy is expanding rapidly worldwide, being horizontal axis wind turbines the technology of larger installed capacity. Modern multi-MW wind turbines have a torque controller and a collective pitch controller to control their power output, particularly when the wind speed is greater than the rated one, or when it is required to down-regulate the turbines' production. In this work we show results of a validated numerical method [1], based on a Large Eddy Simulation-Actuator Line Model framework, applied to evaluate active power control on a real 7.7MW [2][3] onshore wind farm of Uruguay. We describe the implementation of these controllers in `caffa3d` solver [4] and present the methodology we applied to obtain the controller parameters, such as the gain scheduling of the closed loop Proportional-Integral pitch controller. For validation, the simulation results are compared with 1Hz data obtained from the Supervisory Control and Data Acquisition System of the wind farm, focusing on the temporal evolution of the following variables: wind velocity, rotor angular speed, pitch, aerodynamic and electric torque and power. We analyze the Active Power Control response under different de-rate signals, both constant and time-varying, and subject to two wind profiles and two different wind directions, one of them with significant influence of wakes on one wind turbine. The dependence of the wake on the de-rate value is also evaluated, assessing the streamwise velocity component and the turbulence intensity in the wake.

## 1. Introduction

There has been a significant development of methods and tools for performing high fidelity simulations of wind flow through wind turbines applied to real wind farms, providing useful data for the stages of design or operation of wind farms, within the Large Eddy Simulation (LES) alongside with Actuator Models, such as the Actuator Disk (ADM) or the Actuator Line Model (ALM) [5][6][7] for representing the wind turbines rotors. Recently, the authors presented an application of the LES-ALM methodology, simulating a real wind farm under various wind conditions [2], validating the results with Supervisory Control and Data Acquisition (SCADA) system, and also a wind tunnel experimental setup, evaluating the performance and wakes of three model wind turbines with a non-greedy yaw setting [1] [8] .

As in many parts of the world, in Uruguay there has been a significant increase in the penetration level of wind energy in the utility power grid, reaching an installed capacity of over 1500MW, representing 70% of the peak power demand. This fact, together with the uncertainty of the power output of a wind farm, caused among other factors by the variability of the wind flow within a wind farm, makes it more difficult for the transmission system operator (TSO) to regulate the power grid. These facts motivate research about wind farms' ability to provide grid

balancing services, as primary and secondary frequency regulation, as there will be an increasing need for this ancillary service. One method of providing this service is active power control (APC), in which the wind farm should track a power reference signal provided by the TSO, with the objective of helping to balance the total power generated with the power consumed on the grid [9][10].

The implementation of the wind turbine torque and pitch controllers in the CFD code `caffa3d` [4][11], with the aim of regulating active power, was presented in [12]. In that work, an arrangement of two semi-aligned wind turbine models, operating above-rated wind speed, was simulated, comparing the numerical results with data obtained from a state-of-the-art wind tunnel campaign. Continuing with this line of research, the aim of the present paper is to show numerical results of the operation of wind turbines under APC. Some results are compared with high frequency SCADA data considered at specific dates, in order to validate them. With this purpose the 7.7MW onshore wind farm 'Libertad', the same as in [2] [3], was simulated, considering two atmospheric boundary layers (ABL) as inflow condition as well as two different wind directions, one of them showing strong interactions between the turbines due to their wakes. `Caffa3d` solver is used to simulate the wind flow, representing the wind turbines with the Actuator Line Model (ALM) [13]

The rest of this paper is organized as follows: the next Section presents the simulated wind farm Libertad; Section 3 gives details of the simulation setup, such as the domain and grid characteristics and the inflow conditions considered at the inlet. Section 4 describes the implementation of APC control, including the methodology to estimate the pitch-controller gains, based on the one presented by NREL 5-MW reference wind turbine [14]. In Section 5 the numerical results are shown and discussed, ending with conclusions and future work in Section 6.

## 2. Libertad wind farm

The simulated wind farm is Libertad (Figure 1), the one described in [2][3], a 7.7MW onshore wind farm located in the south of Uruguay, which has been operated since August 2014 by the Uruguayan company Ventus ([www.ventusenergia.com](http://www.ventusenergia.com)). It consists of four Vestas V100 wind turbine generators (WT), with rated rotor speed ( $\omega_0$ ) of 14.9RPM, two with rated power ( $P_{rated}$ ) of 1.9MW (WT1 and WT2) and two of 1.95MW (WT3 and WT4), all four with a hub height of 95m and a rotor diameter of 100m. The farm has a meteorological mast with anemometers at 95m, 80m and 60m, and wind vanes at 93m and 58m height. The terrain surrounding the wind turbines is mostly flat, with no significant slopes according to annex B of IEC 61400-12-1 Standard.

Data acquired by the SCADA system of the turbines is recorded on a 1 Hz frequency basis, at selected periods of time and compared with the simulations' results. For this work we consider the temporal evolution of the following 5 signals of each turbine: electric power, aerodynamic and electric torque, wind speed, rotor angular speed and blades pitch-angle. Also, ten-minutes mean and standard deviation of several signals are available for the whole period of operation of the wind farm. The mean free wind velocity and direction is computed from the ten-minutes averages measured at the meteorological mast at the same time periods. It is worth mentioning that the electric and aerodynamic torque are not directly measured by the SCADA system, so we estimate them according to Eq. (1) and Eq. (3), considering the electric power and rotor speed measured signals.

## 3. Numerical Setup

`Caffa3d.MBRi` [4][11] is an open source, finite volume (FV) code, second order accurate in space and time, parallelized with Message Passage Interface (MPI), in which the domain is divided in unstructured blocks of structured grids. The ALM has been implemented in the code [15] to

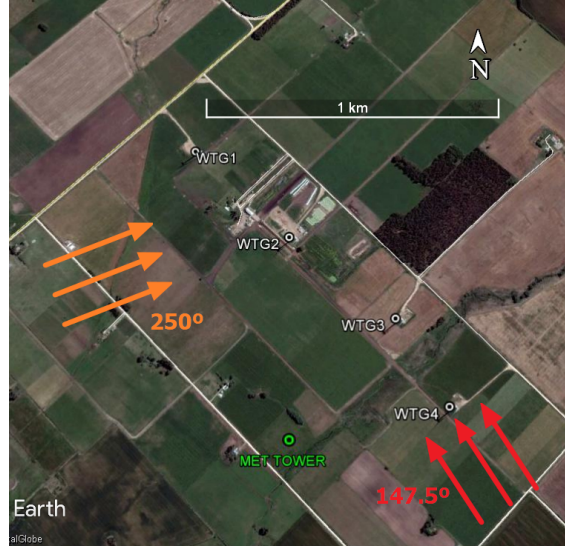


Figure 1: Libertad wind farm layout. The arrows indicate the simulated wind directions.

represent wind turbines rotors in the simulations. For further information about the code and its application in wind energy, please see [2][3][16][17][18][19].

The size of the computational domain is the same as in [3], considering the middle grid resolution (R1) described in that paper. Two different ABL wind profiles, which are obtained from precursor simulations as described in [2] [3], are considered at the inlet of the domain. The span-wise average of the mean stream-wise velocity component at hub height ( $V_{HH}$ ) is 9m/s and 12.6m/s and the stream-wise turbulence intensity is 9.1% and 7.8% respectively. The inlets are referred as 9m/s and 12m/s in future sections of this work. Figure 2 depicts the velocity and turbulence intensity span-wise average profiles of both precursor simulations.

The Crank-Nicolson scheme is used to advance in time, with a temporal step set at 0.25s and the scale-dependent dynamic Smagorinsky model, to compute the subgrid scale stress. To represent the wind turbine rotor, the ALM is used the same way as in [3]. The presence of the tower and nacelle are taken into account through drag coefficients, in a similar approach as presented in [20]. The chord and twist angles as well as the airfoil's data, and the relationship between the rotational speed of the rotor and its torque are taken from [3]. At each time step of the simulation, the rotational speed is obtained from the rotor momentum balance equation (1), where  $M_{gen}$  is the generator torque,  $\omega$  is the angular speed of the rotor at the current time step,  $I$  is the sum of the inertias of the rotor, shaft and generator, considered at the low-speed side.  $\Delta t$  corresponds to the temporal step and  $\omega_{t-1}$  accounts for the rotational speed of the previous time step.

$$I \frac{d\omega}{dt} = M_{aero} - M_{gen} \Rightarrow \omega_t = \frac{(M_{aero_t} - M_{gen_t})}{I} \Delta t + \omega_{t-1} \quad (1)$$

The inertia was estimated taking into account the rotor diameter, the material it is made of and the wind turbine rated power [21], obtaining a value of  $I = 1.72 \times 10^7 \text{ kgm}^2$ . Finally, the aerodynamic and electric power are calculated as the rotational speed multiplied by the shaft aerodynamic torque and the generator torque, Eq. (2 and Eq. (3) respectively.

$$P_{aero} = M_{aero} \cdot \omega \quad (2)$$

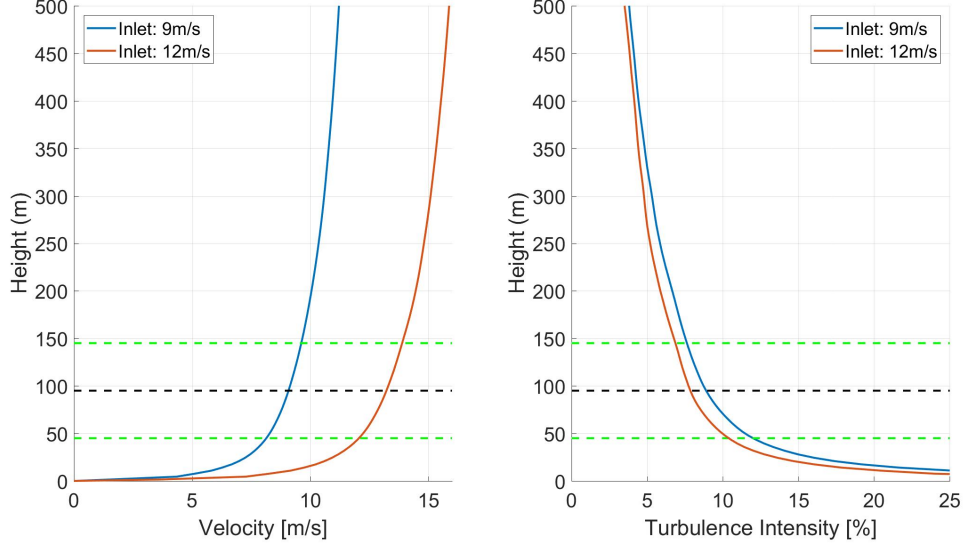


Figure 2: Stream-wise velocity component and turbulence intensity at the inlet of the simulations. The dashed black and green lines represent the hub and blade tips positions respectively.

$$P_{electric} = M_{gen} \cdot \omega \quad (3)$$

#### 4. Power controllers

A power control system was implemented in the code, in the same manner as described in [12], which in turn is based on the NREL 5MW reference wind turbine [14]. It consists of two control systems which work independently, the generator torque ( $M_{gen}$ ) and the blade-pitch ( $\theta$ ) controllers.

##### 4.1. Generator torque controller

At the below-rated rotor speed range, referred to as region 2, the objective is to maximize power capture [22]. When the rotor speed is below  $0.9 \times \omega_0$ , being  $\omega_0$  the rated speed, the equation that governs the generator torque controller is:

$$M_{gen} = K \cdot \omega^2 \quad (4)$$

$\omega$  accounts for the current rotor angular speed and  $K$  is a constant that optimizes the power extraction from the wind and which depends on the aerodynamics and geometrical characteristics of the rotor, defined as Eq. (5), where  $\rho$  is the air density,  $A$  is the area swept by the rotor,  $R$  is the rotor radius,  $CP_{opt}$  is the optimal power coefficient, computed with the Blade Element Momentum method, and  $\lambda_{opt}$  is the optimal tip speed ratio.

$$K = \frac{1}{2} \rho A R^3 \frac{CP_{opt}}{\lambda_{opt}^3} \quad (5)$$

This constant was estimated from the turbines ten-minutes SCADA data, by computing the mean angular speed and mean electric torque at wind speed bins, considering the whole range of wind velocities. The obtained value  $4.38 \times 10^5 \frac{W}{(\frac{rad}{s})^2}$ , which differs 25% with the theoretical

value, obtained with the BEM method. At the simulation the empirical was considered, as we think it was a better representation of the real operation of the turbine, based on real data.

At the above-rated wind-speed range, region 3, the goal is to ensure the power output is at the desired level, for example at rated power or a given fraction of it, regardless of the fluctuations that the rotor speed may have. The conditions to be at region 3 are either that A)  $\omega$  is greater than  $\omega_0$ , or B) the pitch angle is greater than a minimum value, which in our simulated V100 model is  $1^\circ$ . At region 3,  $M_{gen}$  is computed as equation (6).  $M_{gen}$  has an upper bound of  $Sat_{Factor} \times M_{rated}$ , being  $Sat_{Factor} = 1.1$  a saturation factor and  $M_{rated}$  the rated torque (Eq. (7)) [14].

$$M_{gen} = \frac{P_{rated}}{\omega} \quad (6)$$

$$M_{rated} = \frac{P_{rated}}{\omega_0} \quad (7)$$

When none of the conditions to be at region 3 are fulfilled, and  $\omega$  is between  $0.9 \times \omega_0$  and  $\omega_0$ , then  $M_{gen}$  is computed as a linear interpolation between  $M_{rated}$  and  $M_{optimal}$ , according to equation (8), where  $M_{optimal}$  is computed as  $K \times (\omega_0 \times 0.9)^2$ . This region is called 2.5, and is a transition between regions 2 and 3.

$$M_{gen} = M_{rated} + \frac{(M_{rated} - M_{optimal})}{(0.1 \times \omega_0)} \times (\omega - \omega_0) \quad (8)$$

#### 4.2. Blade-pitch controller

This controller operates only at region 3 and its objective is to regulate the generator speed, and thus the rotor angular speed, at the rated operation point. At region 2, the pitch-angle of the blades is fixed at its minimum value,  $-2^\circ$  in order to optimize the power extraction from the wind. This minimum value was obtained from the 10-minute mean of the pitch signal. At regions 2.5 and 3, the rotor-collective blade-pitch-angle values are computed using a proportional-integral (PI) gain-scheduled control on the speed error ( $\Delta\omega$ ) between the current WT speed and the rated speed ( $\omega_0$ ) [14], as shown in equation (9).

$$\theta = K_P \Delta\omega + K_I \int_0^t \Delta\omega dt \quad (9)$$

$\theta$  is the pitch angle,  $K_I$  and  $K_P$  account for the proportional and integral gains respectively. The integral term accounts for the accumulated error over time, and in the simulations it is computed by simply adding  $\Delta\omega$  to its previous value, in each time step. Based on [14],  $K_I$  and  $K_P$  are computed as equation (10).

$$K_P = \frac{2 \cdot I \cdot \omega_0 \cdot \zeta_\varphi \cdot \omega_{\varphi n}}{-\frac{\partial P}{\partial \theta}} \quad ; \quad K_I = \frac{I \cdot \omega_0 \cdot (\omega_{\varphi n})^2}{-\frac{\partial P}{\partial \theta}} \quad (10)$$

The blade-pitch sensitivity,  $\frac{\partial P}{\partial \theta}$ , is an aerodynamic property of the rotor that depends on the wind speed, rotor speed, and blade-pitch angle. It was estimated with the BEM method, computing the difference in aerodynamic power by considering small variations of the pitch angle around its optimal value, for various wind speeds. As suggested in [14] we invoke the frozen-wake assumption, in which the induced wake velocities are held constant while the blade-pitch angle is perturbed. To validate this methodology we also computed it for the 5MW reference wind turbine, taking into account the published data in [14]. Figure 3 shows these results, showing very good agreement with the NREL turbine.

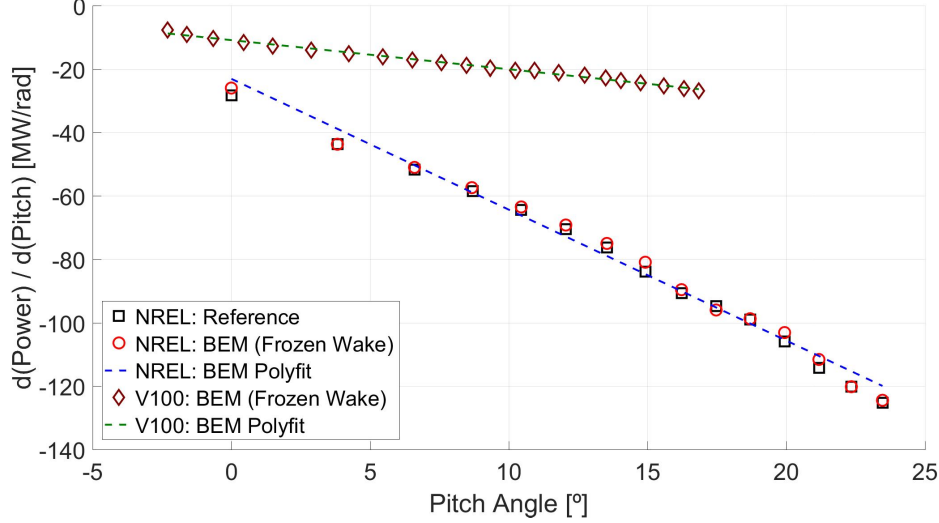


Figure 3: Blade-pitch sensitivity of the Vestas V100 and 5MW NREL wind turbines.

As it can be observed, the pitch sensitivity, varies nearly linearly with blade-pitch angle, so a linear fit was computed, obtaining:

$$\frac{\partial P}{\partial \theta}(\theta = 0) = -1.025 \times 10^7 \frac{W}{rads} \quad \text{and} \quad \theta_{KK} = 11.8 \quad (11)$$

where  $\theta_{KK}$  is the blade-pitch angle at which the pitch sensitivity has doubled from its value at  $(\theta = 0)$ . Considering these values, as well as  $\omega_{\varphi n} = 0.7$  and  $\zeta_{\varphi} = 0.1$  the obtained gains are:  $K_P(\theta = 0) = 0.314s$ ;  $K_I(\theta = 0) = 0.942$ . The gain-correction factor, which multiplies each gain and depends on the blade-pitch angle is computed as:

$$GK(\theta) = \frac{1}{1 + \frac{\theta}{\theta_{KK}}} \quad (12)$$

Based on SCADA data and [14], the pitch-angle is limited by saturation values, of  $[-2^\circ, +90^\circ]$  and its maximum rate of change is set to  $8^\circ/s$ . This PI controller ensures that  $\omega$  fluctuates around its reference value, and so the active power output fluctuates around the active power rated value,  $P_{rated}$ .

#### 4.3. Active Power Control

If there is enough wind velocity, a way to track a power reference signal given by the TSO can be to de-rate the wind turbines from their rated power. To accomplish this, three de-rating modes are proposed in [9][10]: 1) capturing a fraction of the rated power, 2) maintaining a constant power reserve, as a fraction of the rated power and 3) producing a fraction of the available power. At the present work only the first mode is considered. For the other two modes a estimation of the available power is required. For the selected mode, the generator torque controller is the same as presented in sub-section 4.1, but applying an upper bound to  $M_{gen}$  of  $Sat_{Factor} \times M_{DR}$ , instead of  $Sat_{Factor} \times M_{rated}$ .  $M_{DR}$  is computed considering the de-rating command ( $DRd$ ) required by the TSO (Equation 13).

$$M_{DR} = \frac{P_{rated}}{(\omega_0)^2} \times DR \quad (13)$$

This mode is simply an extension of the controllers presented in the previous sub-sections 4.1 and 4.2, where the wind turbine, when it is operating at region 3, limits its power production to the required value when there is enough wind velocity, regulating the aerodynamic torque with the blade-pitch controller. When there is not enough wind to generate the required power, the wind turbine operates at region 2, optimizing the power extraction from the wind by regulating the rotor speed with the generator torque controller.

In the simulations  $DR$  can be a constant signal or vary over time, but it needs to be specified for each wind turbine individually, prior to the execution of the simulation. In the near future it is planned to implement a wind plant global controller, to coordinate the actions of the individual turbines, accounting for the interactions of wakes based, for example, on the available power of each turbine, as in [23] or [24].

## 5. Results and discussion

In this section the results of the simulations are presented, focusing on the temporal evolution of the controller signals: aerodynamic and electric torque, power, rotor speed, wind speed and pitch angle. In the first place, we performed simulations without considering any de-rate commands applied to the turbines. Numerical results of selected wind turbines are compared to 1Hz SCADA data on a specific period, in order to validate the controllers. Secondly, we presented only numerical results, considering several de-rate signals, another wind speed profile, as described in Section 3 and different wind directions, to evaluate the effect of wake interaction in the power control. Also results of the total production of the wind farm are shown, comparing 3 constant de-rate signals. Finally, a single wind turbine simulation was performed, without considering topography, to evaluate the effect of de-rating a wind turbine on its wake.

### 5.1. Controllers validation

Figure 4a depicts the temporal evolution of 1200 seconds simulation and SCADA data of WT3. The SCADA data corresponds to a period starting on the 23rd November 2017 at 12.30hs, when the average wind speed and wind direction were 12.5m/s and  $264^\circ$  respectively, according to the meteorological mast measurements. Figure 4b shows the same signals for WT2, comparing with SCADA data acquired on 5th May 2018, when the wind direction average was  $310^\circ$  and the wind speed 13m/s. The wind direction considered at the simulation was  $250^\circ$ . It is worth noting that in none of these directions ( $250^\circ$ ,  $264^\circ$  and  $310^\circ$ ) the wind farm turbines are affected by the wake of another turbine, and as the wind speed was similar in both periods, no significant differences were noticed in the operation of the turbines.

The shown signals are wind speed, rotor angular speed, pitch angle and aerodynamic and electric power. The simulation wind speed signal corresponds to the value at the cell located at the inlet of the domain, at hub height and just upstream of the corresponding wind turbine position; the SCADA signal is the velocity measured at the wind turbine nacelle. Good agreement can be seen between the simulation and the SCADA data in all the signals. It can be noticed that the oscillations in the aerodynamic torque are significantly larger than in the electric torque, both for the simulation and SCADA variables. In the simulation signals, peaks at a frequency of 0.75Hz can be observed, which is equal to 3 times the frequency associated to  $\omega_0$ , and is due to the passage of the blades in front of the tower. The difference between the electric and aerodynamic torque is what causes the acceleration and deceleration of the rotor. The pitch signals also show good agreement, taking values above the minimum during all the 1200s period, which shows that pitch-controller is operating to regulate the power output. Significant peaks can be observed in the electric power SCADA signals during a few seconds, but this paper does not focus on them. We assume they are caused by the operation of electric components (e.g the inverter or the generator), which we do not consider in our simulation. The gray zone at the beginning of the time series represents the first 200 seconds, and indicates the

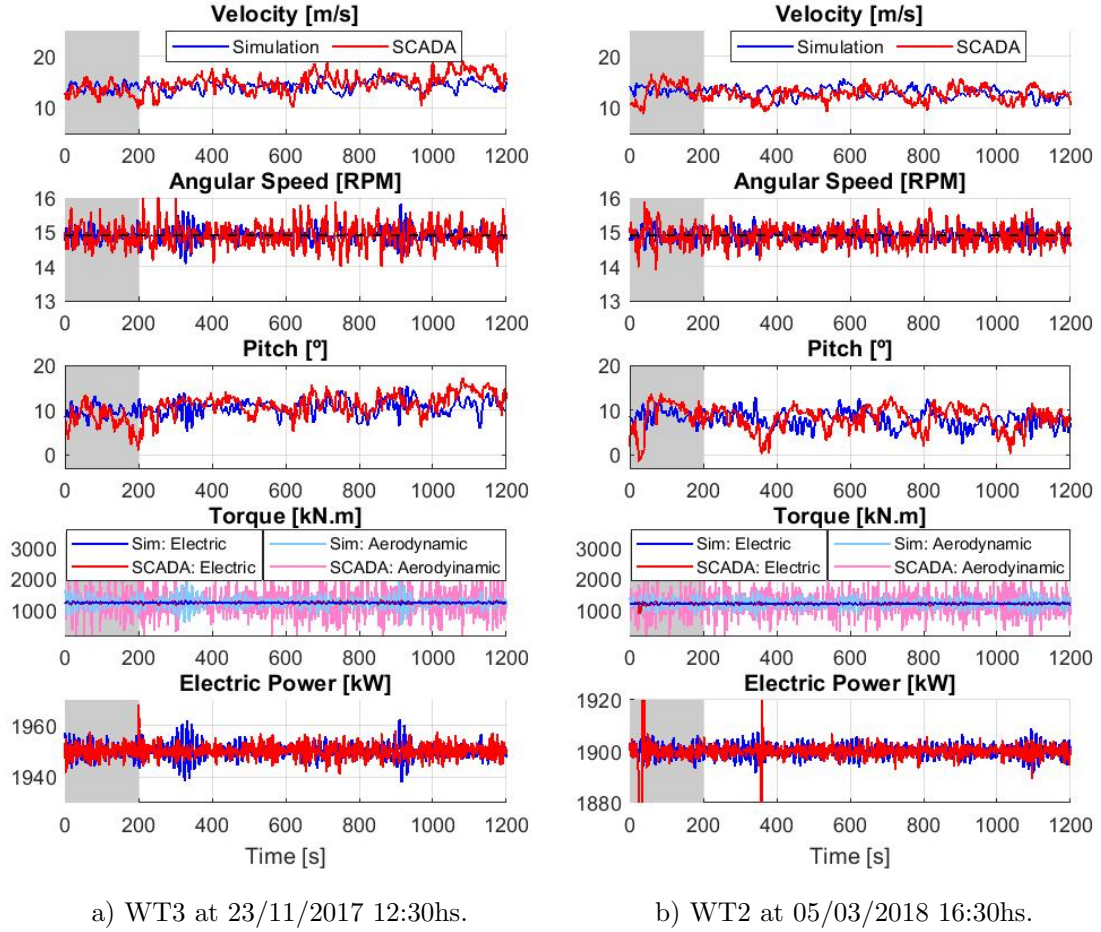


Figure 4: Simulation results and high frequency SCADA data. The gray area indicates transients effects at the beginning of the simulations.

period affected by transient effects, such as the development of the wakes, due to the sudden inclusion of the turbines in the simulations.

### 5.2. Active Power Control at wind turbine level

We performed simulations considering several de-rate values for each turbine, another wind direction and a different ABL velocity profile at the inlet. The following figures of this Section depict numerical results of the temporal evolution of WT3 and WT4 signals. These turbines were chosen because WT3 performance was clearly affected by WT4 wake at the 147° wind direction simulation (see Figure 1).

Figure 5 compares results of WT3 operation at 250° and 147° with wind speed at the inlet and hub height of 12m/s. Two constant de-rate commands are considered: 100% (equivalent to rated power, Figure 5) and 60% (Figure 6). For both wind directions, as there is enough wind velocity to reach rated power, the required levels of electric power can be accomplished, as it can be seen in the bottom subplot of the figure, while the rotor speed oscillates around its rated value in all cases. Regarding the pitch angle, higher values are observed at wind direction 250° than at 147° because in the latter WT3 is at the wake of WT4 and, therefore, with less available

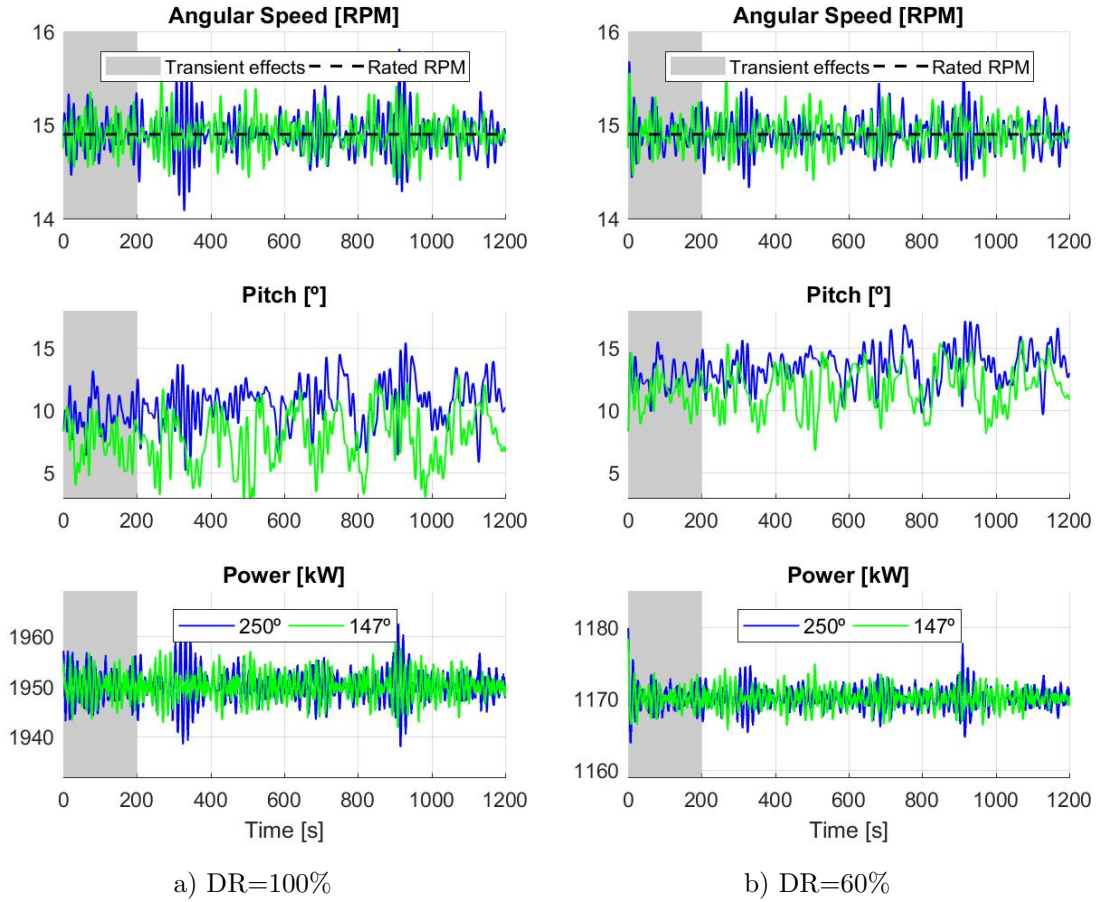


Figure 5: WT3 operation at  $Dir = 147^\circ$  and  $Dir = 250^\circ$ ;  $V_{HH} = 12m/s$  at inlet and hub height.

power. Also higher pitch values are adopted for de-rate command 60% than for 100%, for the same wind direction (e.g.  $250^\circ$ ), as it is expected.

Figure 6 shows the operation of WT3 and WT4 respectively, at  $147^\circ$  for the other wind profile described in Section 3, with span-wise averaged velocity of  $9m/s$  at hub height, considering 6 de-rate commands for both wind turbines: 100%, 90%, 80%, 70%, 60% and 50%. In the case of WT3, which is at the wake of WT4, it is clearly noticed that the turbine does not reach the required de-rated power, except for some moments with  $DR=50\%$  and  $DR=60\%$ , when there is enough available power on the wind flow. Also, it can be noticed that the power production of WT3 decreases with higher de-rate values of WT4, as there is less available power due to its wake. The angular speed is regulated and the pitch angle is kept constant at its minimum value most of the time. In the case of WT4, the required power is reached in all de-rate levels, although for  $DR=100\%$ ,  $90\%$  and  $80\%$  there are periods where the angular speed does not reach rated value, and thus the generator torque controller operates at region 2, regulating rotor speed to optimize the power extraction from the wind. Again, for lower de-rate commands, higher pitch angles are adopted. In these situations, the transient effects at the beginning of the simulation can be clearly observed in the angular speed, pitch and power signals, showing the wake propagation of WT4.

Figure 7 depicts the total wind farm power output, comparing three de-rate levels, for case

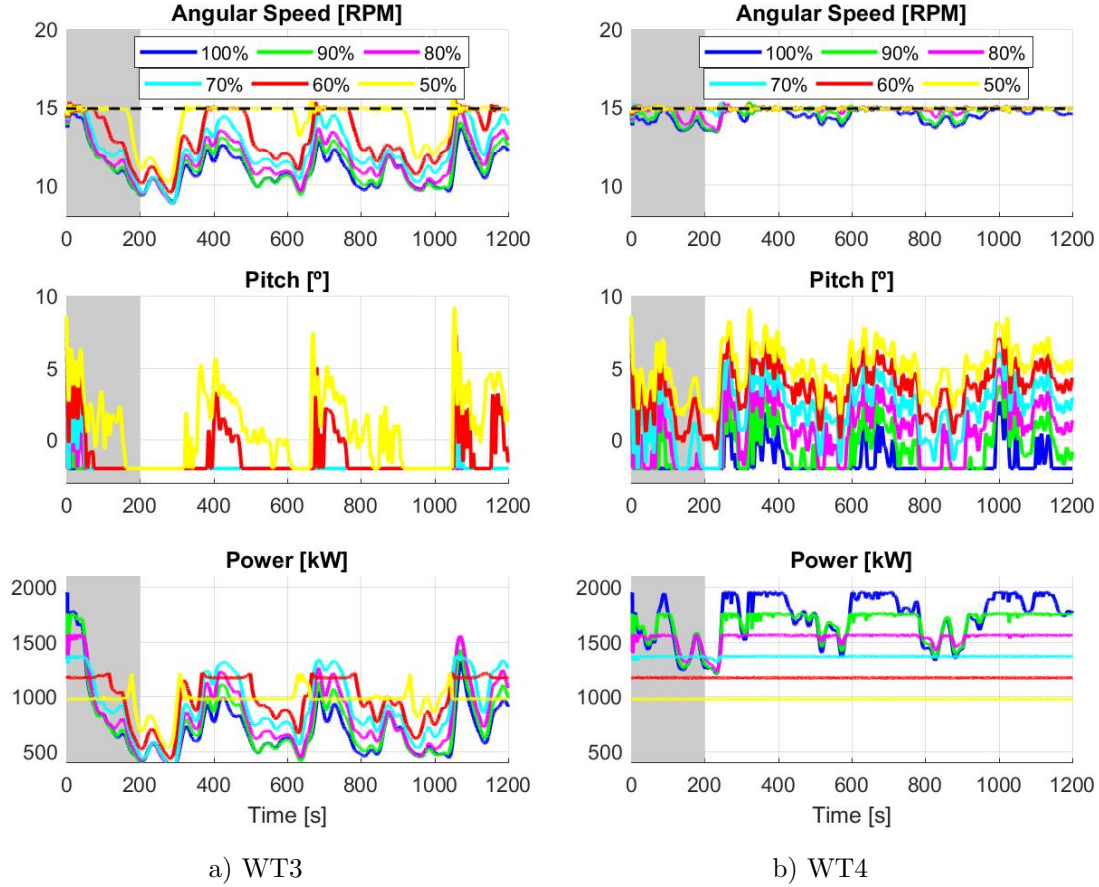


Figure 6: WT3 and WT4 operation at  $Dir = 147^\circ$  ;  $V_{HH} = 9m/s$  at inlet and hub height.

$Dir = 147^\circ$  and  $V_{HH} = 9m/s$ . The de-rate commands are equally distributed to each turbine, regardless of their capacity to reach the desired power. As it can be seen, only in the case of DR=50% the required level is reached most of the time. In the other simulations, the power is not reached mainly because WT3 does not reach its required power as it is strongly affected by WT4 wake. These results show the need to implement a global wind farm controller, with the purpose of assigning de-rate commands based on the available power of each wind turbine, especially when there are turbines operating in the wake of others. Different types of global controllers were studied in [23] and [24], where they evaluate the effect of considering an open-loop or a closed-loop global controller, on the total power.

The response of the controller under different time-varying de-rate signals was evaluated: a step type signal, which changes its DR value every 300s, from 80%, 50%, 100%, to 70%; and a sinusoidal signal of frequency  $2.5 \times 10^{-5}$ , which oscillates between  $P_{rated}$  and  $0.4 \times P_{rated}$ , but those results are not shown here. Although the aerodynamic power presented significant oscillations, the electric power followed the required signal shape. It is worth mentioning that the electric power presents minor oscillations, of around 5%, which can be observed in Figure 5, with a zoomed scale. In future work it is planned to evaluate the response of a whole wind farm subject to APC signals that are typically required by the TSO, in order to provide ancillary services, e.g. contributing to the system frequency regulation.

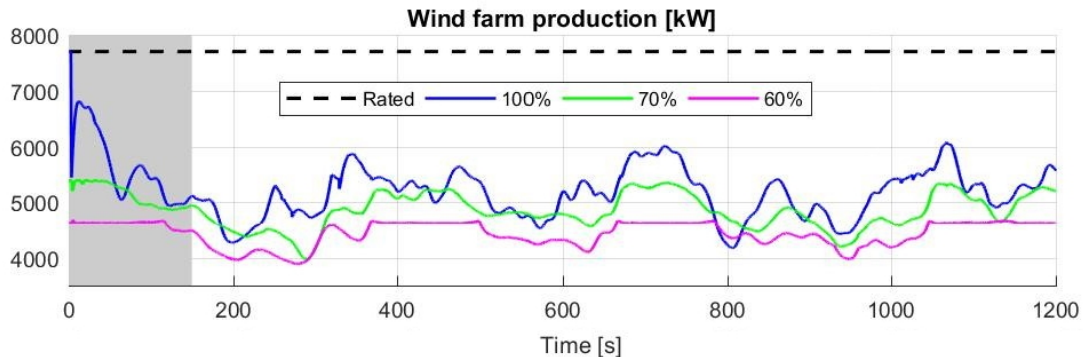


Figure 7: Power production of the wind farm (top) and each individual WT operating at 3 constant different de-rate commands, at  $Dir = 147^\circ$ ;  $V_{HH} = 9m/s$  at inlet and hub height.

### 5.3. Wake characteristics of a down-regulated wind turbine

Finally, the dependence of the velocity deficit and turbulence intensity on the wake, with respect to the de-rate value, was evaluated. For this, we simulated the operation of a single wind turbine subject to the ABL profile with 9m/s at hub height on flat terrain. Figure 8 depicts profiles of the mean stream-wise velocity component ( $U$ ) and turbulence intensity of the stream-wise velocity component ( $TI_U$ , see Eq. (14)), in a horizontal plane at hub height.

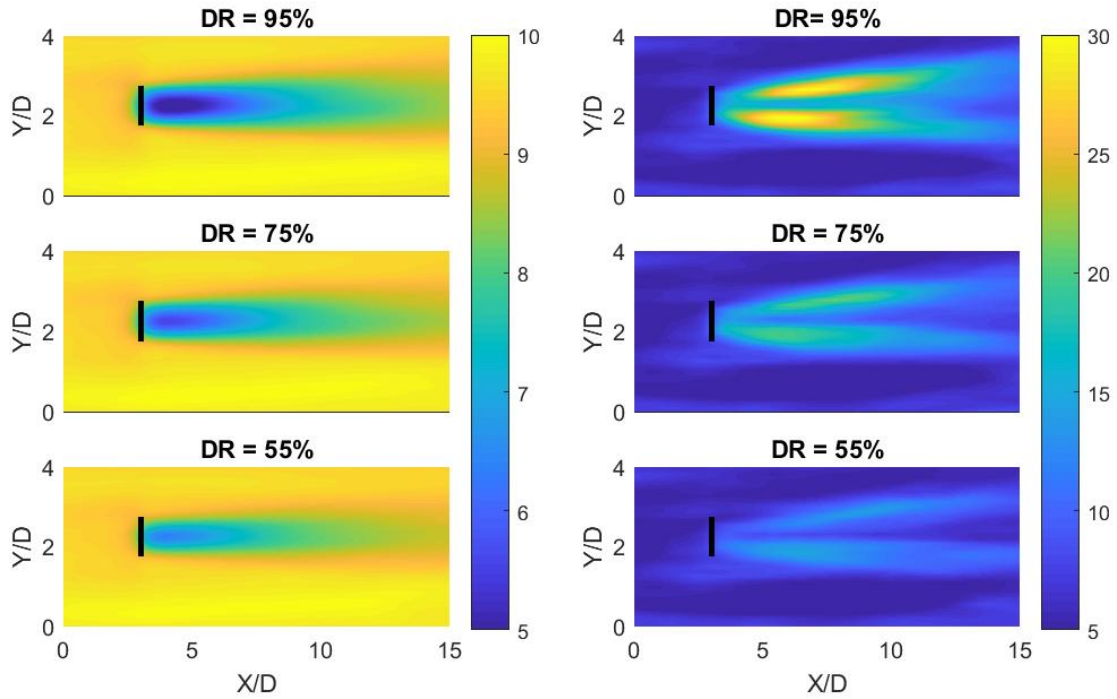
$$TI_U = \frac{\sigma_u}{\langle U \rangle} \quad (14)$$

As expected, the wake velocity deficit increases with higher de-rate commands, as the turbine extracts more power from the wind flow, and causes higher turbulence intensity. The maximum turbulence intensity is obtained between 3D and 5D from the rotor plane, similar to the results presented in [1][17][20]

## 6. Conclusions and future work

A Large Eddy Simulation framework with the Actuator Line Model to represent the wind turbine rotors has been used to simulate the operation of a 7.7MW onshore wind farm. The simulations considered two different ABL wind profiles, with hub height velocities close or higher than the rated one, and also considered two different wind directions, one of them with strong interaction between wakes and wind turbines. A closed-loop collective-pitch and a torque controller was implemented in the CFD code based on the one presented in [14] The results of the simulations were compared to high frequency data (1Hz) from the SCADA system, obtaining good agreement, both in the mean values and the temporal evolution of the signals.

The response of the controller subject to different de-rate values, both constant and time-varying, was evaluated. We show that when there is enough wind power in the flow, the individual wind turbines can follow the required signal, but when it comes to the total wind farm power output, it fails to accomplish what is required. because of the interaction between wakes and turbines. These results shows the necessity of implementing a global controller, which takes into account the available power of each wind turbine. We plan to work on it in the near future. In this sense, a preliminary evaluation of the dependence of the wake shape on the de-rate signal, was performed, and further investigation on this subject will be useful to determine the available power of each individual turbine.



a) Mean stream-wise velocity component ( $U$ )      b) Mean turbulence intensity ( $TI_U$ )

Figure 8:  $U$  (left) and  $TI_U$  (right) horizontal planes at hub-height. Single wind turbine operating with 3 different de-rate commands.  $V_{HH} = 9m/s$  at inlet and hub height.

Besides, the use of GPU computing platform as considered in [25] is now being expanded to the full flow solver, using a dual CUDA/OpenCL syntax on top of the coarse MPI parallelization. This approach allows achieving speedups of up to 30x with respect to the CPU only solver and will be next extended to the wind turbine module routines.

## References

- [1] M.Draper, A.Guggeri, M.Mendina, G.Usera, and F.Campagnolo. Journal of Wind Engineering & Industrial Aerodynamics A Large Eddy Simulation-Actuator Line Model framework to simulate a scaled wind energy facility and its application. 182(September):146–159, 2018.
- [2] A.Guggeri, D.Slamovitz, M.Draper, and G.Usera. A High-Fidelity Numerical Framework For Wind Farm Simulations. *Tenth International Conference on Computational Fluid Dynamics (ICCFD10)*, pages 1–13, 2018.
- [3] A.Guggeri, M.Draper, and G.Usera. Simulation of a 7.7 MW onshore wind farm with the Actuator Line Model. *Journal of Physics: Conference Series*, 854(1), 2017.
- [4] M.Mendina, M.Draper, A. P.Kelm Soares, G.Narancio, and G.Usera. A general purpose parallel block structured open source incompressible flow solver. *Cluster Computing*, 17(2):231–241, 2014.
- [5] P. K.Jha, M. J.Churchfield, P. J.Moriarty, and S.Schmitz. Accuracy of state-of-the-art actuator-line modeling for wind turbine wakes. *AIAA Paper*, (2013-0608), 2013.
- [6] R. J. A. M.Stevens, L. A.Martinez-Tossas, and C.Meneveau. Comparison of wind farm large eddy simulations using actuator disk and actuator line models with wind tunnel experiments. *Renewable Energy*, 116:470–478, 2018.
- [7] L. A.Martinez-Tossas, M. J.Churchfield, and S.Leonardi. Large eddy simulations of the flow past wind turbines: actuator line and disk modeling. *Wind Energy*, 18(6):1047–1060, 2014.
- [8] M.Draper, A.Guggeri, B.López, A.Díaz, F.Campagnolo, and G.Usera. A Large Eddy Simulation framework

- to assess wind farm power maximization strategies: Validation of maximization by yawing. In *Journal of Physics: Conference Series*, volume 1037, 2018.
- [9] J.Aho, A.Buckspan, L. Y.Pao, and P. A.Fleming. An Active Power Control System for Wind Turbines Capable of Primary and Secondary Frequency Control for Supporting Grid Reliability. *AIAA/ASME Wind Symposium*, (January):1–13, 2013.
- [10] J.Aho, P.Fleming, and L. Y.Pao. Active power control of wind turbines for ancillary services: A comparison of pitch and torque control methodologies. *2016 American Control Conference (ACC)*, pages 1407–1412, 2016.
- [11] G.Usera, A.Vernet, and J. A.Ferré. A Parallel Block-Structured Finite Volume Method for Flows in Complex Geometry with Sliding Interfaces. *Flow, Turbulence and Combustion*, 81(3):471, 2008.
- [12] A.Guggeri, M.Draper, G.Usera, and F.Campagnolo. An Actuator Line Model Simulation of two semi-aligned wind turbine models, operating above-rated wind speed. In *Journal of Physics: Conference Series*, pages 1–14, 2018.
- [13] J. N.Sorensen and W. Z.Shen. Numerical Modeling of Wind Turbine Wakes. *Journal of Fluids Engineering*, 124(2):393, 2002.
- [14] J.Jonkman, S.Butterfield, W.Musial, and G.Scott. Definition of a 5-MW reference wind turbine for offshore system development. Technical report, National Renewable Energy Laboratory (NREL), Golden, CO., 2009.
- [15] M.Draper. *Simulación del campo de vientos y de la interacción entre aerogeneradores*. PhD thesis, 2015.
- [16] M.Draper and G.Usera. Evaluation of the Actuator Line Model with coarse resolutions. *Journal of Physics: Conference Series*, 625(1):12021, 2015.
- [17] M.Draper, A.Guggeri, and G.Usera. Validation of the Actuator Line Model with coarse resolution in atmospheric sheared and turbulent inflow. *Journal of Physics: Conference Series*, 753:82007, sep 2016.
- [18] M.Draper, A.Guggeri, and G.Usera. Modelling one row of Horns Rev wind farm with the Actuator Line Model with coarse resolution. *Journal of Physics: Conference Series*, 753:82028, sep 2016.
- [19] M.Draper, A.Guggeri, M.Mendina, G.Usera, and F.Campagnolo. A Large Eddy Simulation model for the study of wind turbine interactions and its application. In *10th International Conference on Computational Fluid Dynamics*, Barcelona, Accepted for presentation, 2018.
- [20] Y.-T.Wu and F.Porté-Agel. Large-Eddy Simulation of Wind-Turbine Wakes: Evaluation of Turbine Parametrisations. *Boundary-Layer Meteorology*, 138(3):345–366, 2010.
- [21] A. G.González Rodríguez, A.González Rodríguez, and M.Burgos Payán. Estimating Wind Turbines Mechanical Constants. volume 1, pages 9–11, 2007.
- [22] M. O.Hansen. *Aerodynamics of Wind Turbines*. 2008.
- [23] P.Fleming, J.Aho, P.Gebraad, L.Pao, and Y.Zhang. Computational Fluid Dynamics Simulation Study of Active Power Control in Wind Plants. *American Control Conference*, pages 1413–1420, 2016.
- [24] J. W.van Wingerden, L.Pao, J.Aho, and P.Fleming. Active Power Control of Waked Wind Farms. *IFAC-PapersOnLine*, 50(1):4484–4491, 2017.
- [25] P.Igounet, P.Alfaro, G.Usera, and P.Ezzatti. Towards a finite volume model on a many-core platform. *International Journal of High Performance Systems Architecture* 12, 4(2):78–88, 2012.

# Bibliography

- [1] Global Wind Energy Council. Global wind energy outlook. Technical report, 2016.
- [2] Global Wind Energy Council. Annual Market Update 2017. Technical report, 2017.
- [3] Martin O.L Hansen. *Aerodynamics of Wind Turbines*. 2008.
- [4] AUDEE Resumen anual. Technical report, 2017.
- [5] El País. <https://negocios.elpais.com.uy/noticias/eolica-principal-fuente-generacion-primera-vez.html>, 2018.
- [6] G Usera, A Vernet, and J A Ferré. A Parallel Block-Structured Finite Volume Method for Flows in Complex Geometry with Sliding Interfaces. *Flow, Turbulence and Combustion*, 81(3):471, 2008.
- [7] Mariana Mendina, Martin Draper, Ana Paula Kelm Soares, Gabriel Nancio, and Gabriel Usera. A general purpose parallel block structured open source incompressible flow solver. *Cluster Computing*, 17(2):231–241, 2014.
- [8] M Draper. *Simulación del campo de vientos y de la interacción entre aerogeneradores*. PhD thesis, 2015.
- [9] M Draper and G Usera. Evaluation of the Actuator Line Model with coarse resolutions. *Journal of Physics: Conference Series*, 625(1):12021, 2015.
- [10] M Draper, A Guggeri, and G Usera. Validation of the Actuator Line Model with coarse resolution in atmospheric sheared and turbulent inflow. *Journal of Physics: Conference Series*, 753:82007, sep 2016.

- [11] A Guggeri, M Draper, and G Usera. Simulation of a 7.7 {MW} onshore wind farm with the Actuator Line Model. *Journal of Physics: Conference Series*, 854:12018, may 2017.
- [12] A Guggeri, D Slamovitz, M Draper, and G Usera. A High-Fidelity Numerical Framework For Wind Farm Simulations. In *Journal of Physics: Conference Series*, pages 1–13, 2018.
- [13] A Guggeri, M Draper, G Usera, and F Campagnolo. An Actuator Line Model Simulation of two semi-aligned wind turbine models, operating above-rated wind speed. In *Journal of Physics: Conference Series*, pages 1–14, 2018.
- [14] A Guggeri, M Draper, and G Usera. Actuator Line Model simulations to study active power control at wind turbine level. *Abstract submitted for presentation at Wake Conference 2019*, pages 1–13.
- [15] M. Draper, A. Guggeri, B. López, A. Díaz, F. Campagnolo, and G. Usera. A Large Eddy Simulation framework to assess wind farm power maximization strategies: Validation of maximization by yawing. In *Journal of Physics: Conference Series*, volume 1037, 2018.